ical techniques included the following: 1) many AVs and GROD-like inclusions occupied neuronal perikarya at terminal stages of CD−/− and CB−/−CL−/− mouse brains; 2) like CD−/− brains, neurons and microglial cells in CB−/−CL−/− brains showed positive staining of subunit c and autofluorescence; 3) AVs in which GROD-like inclusions, together with part of the cytoplasm, were encircled by double-membrane saccules were often observed in these cathepsin-deficient neurons; 4) massive staining for LC3 was intensely observed in neuronal perikarya and dendrites of these mutant brains; 5) in axons of the corpus callosum of these mutant mice, LC3-positive granules were not co-localized with lamp1, while these AVs were primarily encircled by double-membrane saccules; 6) the ratio of the amounts of LC3-II to LC3-I became distinctly high at the terminal stages of these mutant mice by Western blotting, while no clear changes were detected in the amounts of LC3 mRNA; and 7) LC3 molecules were clearly localized on the membrane of autophagosomes when examined by the SDS-FRL method. Based on these data, neuropathological features of these mutant mice are summarized in Table 1.

Autophagy Is Involved in the Accumulation of Lysosomal Compartments in Neurons of CD−/− and CB−/−CL−/− Mouse Brains

The present study showed that LC3-II predominated in CD−/− and CB−/−CL−/− mouse brains at their terminal stages and LC3-immunopositive AVs accumulated in the perikarya of cathepsin-deficient neurons. Until recently, no study has shown the presence of endogenous LC3 on the membrane of autophagosomes in tissue cells by electron microscopy using the immunogold method, except for the present SDS-FRL method. Indeed, numerous autophagosomes, showing an LC3 signal on their outer membrane, were present in the neuronal perikarya when brain tissue was analyzed by the SDS-FRL method. Because LC3-II is present on the isolation membrane of autophagosomes,[14] these autophagosomes are likely to be nascent (AVi). This notion is also supported by the fact that LC3-positive granules in the perikarya of mutant neurons were often distinct from lamp1-positive lysosomes.

It has been shown that autophagy participates in neurodegenerative disorders such as Huntington's disease,[38–40] Alzheimer's disease,[41–43] Parkinson's disease,[44] and transmitted spongiform encephalopathy.[45–47] The involvement of autophagy has also been demonstrated in lysosomal storage disease such as Pompe's disease.[48,49] The cerebral cortical neurons of CD−/− mouse brains show a new form of lysosomal accumulation disease with a phenotype resembling NCL (Batten disease).[11,12,21] The present morphometric study on these CD−/− neurons revealed that lysosomal compartments including GROD-like inclusions and fingerprint profiles, which are typical hallmarks in NCL neurons, and AVs occupied nearly 42% of the perikaryal volume at P23. The volume density of GROD-like inclusions rapidly increased from P15 to P23, corresponding well with increases in volume densities of AVi and AVd, while nearly half of AVi contained GROD-like inclusions in CD−/− neurons at P23. In cerebral cortical neurons of CB−/−CL−/− brains at P13, GROD-like inclusions and AVs were found to occupy nearly 30% of the perikaryal volume, while ~75% of AVi contained GROD-like inclusions. These data strongly support the view that autophagy is involved in the accumulation of lysosomal compartments in CD−/− and CB−/−CL−/− neurons; in particular, GROD-like inclusions are likely to be derived from AVi through AVd.

It has previously been shown that neuropathological features of CB−/−CL−/− mice resemble a lysosomal storage disorder that is distinct from classical NCL and subunit c is not found in accumulated lysosomes of the mutant neurons.[13] However, the present study demonstrated that ultrastructural and morphometric features of CB−/−CL−/− neurons that possessed numerous AVs and GROD-like inclusions were very similar to those of CD−/− neurons. Moreover, immunoreactivity for subunit c and autofluorescence were detected in neurons and F4/80-immunopositive microglial cells of CB−/−CL−/− brains, while neuronal cells in these mutant mouse brains were intensely stained for periodic acid-Schiff. It has been shown that administration of cysteine proteinase inhibitors such as leupeptin and E64 induces the accumulation of lysosomes with ceroid-lipofuscin in brain cells of young rats.[50] At present, it remains unknown whether subunit c is one of common substrates of cathepsins B and L. However, because CB and CL are major cysteine proteinases in lysosomes of neurons and microglial cells,[26] it is reasonable to assume that the loss of these two proteinases in part suppresses the degradation of subunit c in lysosomes of neurons and microglial cells. From these results it seems likely that the pathological configuration of CB−/−CL−/− mice is very similar to that of NCLs.

Moreover, neuropathological features were primarily similar between CD−/− and CB−/−CL−/− mouse brains. In particular, the volume density of GROD-like inclusions was very similar between CD−/− mice at P23 and CB−/−CL−/− mice at P13, indicating that neuropathological damages were much severer in CB−/−CL−/− brains than in CD−/− brains when considering age difference between the two mutant mice. However, fingerprint profiles were not observed in CB−/−CL−/− mouse neurons but in CD−/− mouse neurons. Such a difference may be attributed to the difference in accumulated/undegraded substances in lysosomal compartments between the two mutant mouse neurons.

No accumulation of typical storage lysosomes has been reported in either CB−/− and CL−/− mouse tissue cells, respectively.[18,20] This indicates that CB and CL, respectively, are dispensable in lysosomal proteolysis. In CB−/−CL−/− mouse CNS neurons, however, some common substrates of CB and CL, although unknown at present, are not degraded by other lysosomal proteinases, resulting in the accumulation of GROD-like inclusions and AVs in the neurons. It has been shown that the amount of the LC3-II form is increased in cultured cells treated with chloroquine, which raises pH in lysosomes,[51]

this indicating that autophagy is enhanced in these cells. These lines support the view that the presence of undigested substrates in lysosomes such as subunit c in CD−/− mice and unknown substrates in CB−/−CL−/− mice induces autophagy. In other words, the presence of GROD-like inclusions and AVs with undigested materials such as GROD-like inclusions may be a potent inducer of autophagy in neuronal cells. Until recently, it remains primarily unknown what signaling is essential for autophagosome formation. It has recently been shown that in conditional Atg7-knockout mice in which autophagy is absent specifically in the liver, numerous ubiquitinated aggregates are detected in the cytosol of hepatocytes with the presence of functional proteasomes.[52] This suggests that protein ubiquitination may serve as a signal to the autophagic process in addition to the proteasomes pathway.[52] The presence of ubiquitin-positive inclusion bodies is one of the common pathological characteristics of neurodegenerative diseases including lysosomal storage disorders.[53,54] Therefore, it may be worthwhile to analyze the signaling pathway of autophagosome formation by use of cathepsin-deficient mice in which autophagosomes are abundantly present.

The present RT-PCR study demonstrated that the amounts of the LC3 gene transcript did not vary between cathepsin-deficient and control brains at various stages examined, indicating that changes in amounts of LC3 molecules depend primarily on the posttranslational events. In intact brains, LC3-I was a major form at each stage examined, while the amounts of LC3-II were larger in CD−/− brains at P8, P15, and P23, and in CB−/−CL−/− brains at P13 than those of LC3-I, respectively. It has recently been shown using HeLa cells and primary hepatocytes that, during starvation-induced autophagy, the significant amount of LC3-II is degraded by lysosomal proteinases and increased when inhibited by cysteine and aspartic proteinase inhibitors.[55,56] In other words, LC3 is likely to be a substrate of CD and a common substrate of CB and CL. Moreover, the increase in the LC3 level by such proteinase inhibitors does not occur under nutrient-rich conditions.[55,56] From these lines of evidence, it is possible to assume that the significant increases in amounts of LC3-II in cathepsin-deficient brains at each stage are attributed to the fact that autophagy is facilitated and the degradation of LC3 in autophagolysosomes is in part suppressed.

The Accumulation of Nascent AVs in Axons of the Corpus Callosum Is One of the Pathological Findings of CD−/− and CB−/−CL−/− Mouse Brains

Under various pathological conditions, vacuolar structures with double and single membranes, multilamellar bodies, and dense bodies have been demonstrated to appear in axons of CNS tissues and cultured neurons.[47,57–60] In addition to these ultrastructural analyses and monodansylcadaverine staining for the demonstration of AVs in axons of CNS tissues, the present study showed that AVs found in axons of CD−/− and CB−/−CL−/− mouse brains were immunopositive for LC3 and negative for lamp1 by double immunostaining and primarily encircled by ER-like membrane saccules. These data indicate the followings: 1) there are machineries required for autophagosome formation in axons of brain tissue, 2) AVs in axons of the corpus callosum in CD−/− and CB−/−CL−/− brains are primarily nascent, and 3) the accumulation of AVs in the axons that may correspond well with meganeurites/spheroids could be one of pathological findings in these mutant mouse brains resembling NCLs. These AVs formed in distal axons usually undergo regulated transport back to the cell body, although it remains unknown how and where such nascent AVs in the axons are acidified and the degradation starts. However, the present results showing enormous accumulation of AVs in axons of the mutant neurons suggest that retrograde axonal transport is impeded in these mutant neurons.

Moreover, the present immunohistochemical study on LC3 demonstrated that the accumulation of AVs was also found in dendrites of the cerebellar and cerebral cortical neurons from the cathepsin-deficient mouse brains. These accumulated AVs did not differ from those in the perikarya of neurons from the mutant mouse brains when analyzed by electron microscopy (Supplemental Figure 2 at *http://ajp.amjpathol.org*). Recently, autophagosomes/AVi, multivesicular bodies, multilamellar bodies, and cathepsin-containing autophagolysosomes have been shown to be the predominant organelles and accumulate in large number in dystrophic neurites of brains from Alzheimer's disease.[61] Considering the fact that various types of AVs including cathepsin-positive autophagolysosomes are present in dystrophic neurites,[61] such AVs detected in the case of AD may be different from those in axons of cathepsin-deficient brains and, if anything, resemble those in dendrites of the mutant mouse brains. Although the acidification and transport system may be dependent primarily on disease situations, the accumulation of AVs in the cases of cathepsin-deficient brains is apt to occur earlier and more frequently in axons than in dendrites.

The Conversion of LC3-I to LC3-II and Positive Staining of LC3 Are Also Excellent Markers for Induction of Autophagy in Brains

The behavior of LC3-II has been defined in murine embryonic stem cells,[62] the soleus muscles of chloroquine-treated rats,[51] in rat podocytes,[56] and in embryonic tissue cells of lamp1 and lamp2 double-deficient mice.[63] Based on experiments using transgenic mice systemically expressing LC3 fused to green fluorescent protein (GFP-LC3), it has been proposed that the regulation of autophagy is organ-dependent and the role of autophagy is not restricted to the starvation response.[23] In most peripheral tissue cells, autophagy is distinctly induced under fasting conditions, whereas starvation does not induce autophagy in brain tissue.[23] Although the question of why autophagy is not induced in brain tissue after

starvation has not yet been answered, it is likely that ischemia,[26] proteinase inhibitors such as leupeptin,[60] and lysosomal proteinase deficiencies, as shown in the present study, enhance autophagy activity in CNS neurons. In fact, in GFP-LC3-expressing CD−/− mouse brains, GFP-LC3 was converted from GFP-LC3-I into GFP-LC3-II without interfering the conversion of endogenous LC3-I to LC3-II. More importantly, the accumulation of autophagosomes in CD−/− mouse brains, evidenced by electron microscopy and LC3 immunocytochemistry, was confirmed also by the finding that GFP-LC3-positive granules were accumulated in neuronal perikarya and dendrites of GFP-LC3/CD−/− mouse brains.

Collectively, the current data demonstrate that accumulated lysosomal structures with undigested substrates in neurons of CD−/− or CB−/−CL−/− mouse brains are primarily LC3-immunopositive, suggesting that these structures are derived from autophagosomes and also that autophagy is highly induced in these mutant mouse brains. These lines of evidence suggest that the activation of autophagy plays a pivotal role in the accumulation of lysosomal structures in CNS neurons of mouse models for NCL (Batten disease)/lysosomal storage disorders.

References

1. Klionsky DJ, Emr SD: Autophagy as a regulated pathway of cellular degradation. Science 2000, 290:1717–1721
2. Vittorini S, Paradiso C, Donati A, Cavallini G, Masini M, Gori Z, Pollera M, Bergamini E: The age-related accumulation of protein carbonyl in rat liver correlates with the age-related decline in liver proteolytic activities. J Gerontol A Biol Sci Med Sci 1999, 54:B318–B323
3. Larsen KE, Sulzer D: Autophagy in neurons: a review. Histol Histopathol 2002, 17:897–908
4. Uchiyama Y: Autophagic cell death and its execution by lysosomal cathepsins. Arch Histol Cytol 2001, 64:233–246
5. Yuan J, Lipinski M, Degterev A: Diversity in the mechanisms of neuronal cell death. Neuron 2003, 40:401–413
6. Ohsawa Y, Isahara K, Kanamori S, Shibata M, Kametaka S, Gotow T, Watanabe T, Kominami E, Uchiyama Y: An ultrastructural and immunohistochemical study of PC12 cells during apoptosis induced by serum deprivation with special reference to autophagy and lysosomal cathepsins. Arch Histol Cytol 1998, 61:395–403
7. Hall NA, Lake BD, Dewji NN, Patrick AD: Lysosomal storage of subunit c of mitochondrial ATP synthase in Batten's disease (ceroid-lipofuscinosis). Biochem J 1991, 275:269–272
8. Kominami E, Ezaki J, Muno D, Ishido K, Ueno T, Wolfe LS: Specific storage of subunit c of mitochondrial ATP synthase in lysosomes of neuronal ceroid lipofuscinosis (Batten's disease). J Biochem (Tokyo) 1992, 111:278–282
9. Palmer DN, Martinus RD, Cooper SM, Midwinter GG, Reid JC, Jolly RD: Ovine ceroid lipofuscinosis. The major lipopigment protein and the lipid-binding subunit of mitochondrial ATP synthase have the same NH2-terminal sequence. J Biol Chem 1989, 264:5736–5740
10. Fearnley IM, Walker JE, Martinus RD, Jolly RD, Kirkland KB, Shaw GJ, Palmer DN: The sequence of the major protein stored in ovine ceroid lipofuscinosis is identical with that of the dicyclohexylcarbodiimide-reactive proteolipid of mitochondrial ATP synthase. Biochem J 1990, 268:751–758
11. Koike M, Nakanishi H, Saftig P, Ezaki J, Isahara K, Ohsawa Y, Schulz-Schaeffer W, Watanabe T, Waguri S, Kametaka S, Shibata M, Yamamoto K, Kominami E, Peters C, von Figura K, Uchiyama Y: Cathepsin D deficiency induces lysosomal storage with ceroid lipofuscin in mouse CNS neurons. J Neurosci 2000, 20:6898–6906
12. Nakanishi H, Zhang J, Koike M, Nishioku T, Okamoto Y, Kominami E, von Figura K, Peters C, Yamamoto K, Saftig P, Uchiyama Y: Involvement of nitric oxide released from microglia-macrophages in pathological changes of cathepsin D-deficient mice. J Neurosci 2001, 21:7526–7533
13. Felbor U, Kessler B, Mothes W, Goebel HH, Ploegh HL, Bronson RT, Olsen BR: Neuronal loss and brain atrophy in mice lacking cathepsins B and L. Proc Natl Acad Sci USA 2002, 99:7883–7888
14. Kabeya Y, Mizushima N, Ueno T, Yamamoto A, Kirisako T, Noda T, Kominami E, Ohsumi Y, Yoshimori T: LC3, a mammalian homologue of yeast Apg8p, is localized in autophagosome membranes after processing. EMBO J 2000, 19:5720–5728
15. Ohsumi Y: Molecular dissection of autophagy: two ubiquitin-like systems. Nat Rev Mol Cell Biol 2001, 2:211–216
16. Tanida I, Tanida-Miyake E, Ueno T, Kominami E: The human homolog of Saccharomyces cerevisiae Apg7p is a protein-activating enzyme for multiple substrates including human Apg12p, GATE-16, GABARAP, and MAP-LC3. J Biol Chem 2001, 276:1701–1706
17. Tanida I, Tanida-Miyake E, Komatsu M, Ueno T, Kominami E: Human Apg3p/Aut1p homologue is an authentic E2 enzyme for multiple substrates, GATE-16, GABARAP, and MAP-LC3, and facilitates the conjugation of hApg12p to hApg5p. J Biol Chem 2002, 277:13739–13744
18. Deussing J, Roth W, Saftig P, Peters C, Ploegh HL, Villadangos JA: Cathepsins B and D are dispensable for major histocompatibility complex class II-mediated antigen presentation. Proc Natl Acad Sci USA 1998, 95:4516–4521
19. Saftig P, Hetman M, Schmahl W, Weber K, Heine L, Mossmann H, Koster A, Hess B, Evers M, von Figura K: Mice deficient for the lysosomal proteinase cathepsin D exhibit progressive atrophy of the intestinal mucosa and profound destruction of lymphoid cells. EMBO J 1995, 14:3599–3608
20. Nakagawa T, Roth W, Wong P, Nelson A, Farr A, Deussing J, Villadangos JA, Ploegh H, Peters C, Rudensky AY: Cathepsin L: critical role in Ii degradation and CD4 T cell selection in the thymus. Science 1998, 280:450–453
21. Koike M, Shibata M, Ohsawa Y, Nakanishi H, Koga T, Kametaka S, Waguri S, Momoi T, Kominami E, Peters C, Figura K, Saftig P, Uchiyama Y: Involvement of two different cell death pathways in retinal atrophy of cathepsin D-deficient mice. Mol Cell Neurosci 2003, 22:146–161
22. Saftig P, Peters C, von Figura K, Craessaerts K, Van Leuven F, De Strooper B: Amyloidogenic processing of human amyloid precursor protein in hippocampal neurons devoid of cathepsin D. J Biol Chem 1996, 271:27241–27244
23. Mizushima N, Yamamoto A, Matsui M, Yoshimori T, Ohsumi Y: In vivo analysis of autophagy in response to nutrient starvation using transgenic mice expressing a fluorescent autophagosome marker. Mol Biol Cell 2004, 15:1101–1111
24. Lu Z, Dono K, Gotoh K, Shibata M, Koike M, Marubashi S, Miyamoto A, Takeda Y, Nagano H, Umeshita K, Uchiyama Y, Monden M: Participation of autophagy in the degeneration process of rat hepatocytes after transplantation following prolonged cold preservation. Arch Histol Cytol 2005, 68:71–80
25. Nash JE, Yasumura T: Direct immunogold labeling of connexins and aquaporin-4 in freeze-fracture replicas of liver, brain, and spinal cord: factors limiting quantitative analysis. Cell Tissue Res 1999, 296:307–321
26. Nitatori T, Sato N, Waguri S, Karasawa Y, Araki H, Shibanai K, Kominami E, Uchiyama Y: Delayed neuronal death in the CA1 pyramidal cell layer of the gerbil hippocampus following transient ischemia is apoptosis. J Neurosci 1995, 15:1001–1011
27. Uchiyama Y, Watanabe M: A morphometric study of developing pancreatic acinar cells of rats during prenatal life. Cell Tissue Res 1984, 237:117–122
28. Liou W, Geuze HJ, Geelen MJ, Slot JW: The autophagic and endocytic pathways converge at the nascent autophagic vacuoles. J Cell Biol 1997, 136:61–70
29. Dunn Jr WA: Studies on the mechanisms of autophagy: formation of the autophagic vacuole. J Cell Biol 1990, 110:1923–1933
30. Tanaka Y, Guhde G, Suter A, Eskelinen EL, Hartmann D, Lullmann-Rauch R, Janssen PM, Blanz J, von Figura K, Saftig P: Accumulation of autophagic vacuoles and cardiomyopathy in LAMP-2-deficient mice. Nature 2000, 406:902–906
31. Haltia M: The neuronal ceroid-lipofuscinoses. J Neuropathol Exp Neurol 2003, 62:1–13
32. Koike M, Shibata M, Ohsawa Y, Kametaka S, Waguri S, Kominami E,

Uchiyama Y: The expression of tripeptidyl peptidase I in various tissues of rats and mice. Arch Histol Cytol 2002, 65:219–232
33. Fujimoto K: Freeze-fracture replica electron microscopy combined with SDS digestion for cytochemical labeling of integral membrane proteins. Application to the immunogold labeling of intercellular junctional complexes. J Cell Sci 1995, 108:3443–3449
34. Towbin H, Staehelin T, Gordon J: Electrophoretic transfer of proteins from polyacrylamide gels to nitrocellulose sheets: procedure and some applications. Proc Natl Acad Sci USA 1979, 76:4350–4354
35. Ohsawa Y, Zhang G, Kametaka S, Shibata M, Koike M, Waguri S, Uchiyama Y: Purification, cDNA cloning, and secretory properties of FLRG protein from PC12 cells and the distribution of FLRG mRNA and protein in rat tissues. Arch Histol Cytol 2003, 66:367–381
36. Dunn Jr WA: Autophagy and related mechanisms of lysosome-mediated protein degradation. Trends Cell Biol 1994, 4:139–143
37. Mann SS, Hammarback JA: Gene localization and developmental expression of light chain 3: a common subunit of microtubule-associated protein 1A(MAP1A) and MAP1B. J Neurosci Res 1996, 43:535–544
38. Roizin L, Stellar S, Willson N, Whittier J, Liu JC: Electron microscope and enzyme studies in cerebral biopsies of Huntington's chorea. Trans Am Neurol Assoc 1974, 99:240–243
39. Tellez-Nagel I, Johnson AB, Terry RD: Studies on brain biopsies of patients with Huntington's chorea. J Neuropathol Exp Neurol 1974, 33:308–332
40. Kegel KB, Kim M, Sapp E, McIntyre C, Castano JG, Aronin N, DiFiglia M: Huntington expression stimulates endosomal-lysosomal activity, endosome tubulation, and autophagy. J Neurosci 2000, 20: 7268–7278
41. Cataldo AM, Hamilton DJ, Barnett JL, Paskevich PA, Nixon RA: Properties of the endosomal-lysosomal system in the human central nervous system: disturbances mark most neurons in populations at risk to degenerate in Alzheimer's disease. J Neurosci 1996, 16:186–199
42. Stadelmann C, Deckwerth TL, Srinivasan A, Bancher C, Bruck W, Jellinger K, Lassmann H: Activation of caspase-3 in single neurons and autophagic granules of granulovacuolar degeneration in Alzheimer's disease. Evidence for apoptotic cell death. Am J Pathol 1999, 155:1459–1466
43. Yu WH, Kumar A, Peterhoff C, Shapiro Kulnane L, Uchiyama Y, Lamb BT, Cuervo AM, Nixon RA: Autophagic vacuoles are enriched in amyloid precursor protein-secretase activities: implications for beta-amyloid peptide over-production and localization in Alzheimer's disease. Int J Biochem Cell Biol 2004, 36:2531–2540
44. Anglade P, Vyas S, Javoy-Agid F, Herrero MT, Michel PP, Marquez J, Mouatt-Prigent A, Ruberg M, Hirsch EC, Agid Y: Apoptosis and autophagy in nigral neurons of patients with Parkinson's disease. Histol Histopathol 1997, 12:25–31
45. Boellaard JW, Schlote W, Tateishi J: Neuronal autophagy in experimental Creutzfeldt-Jakob's disease. Acta Neuropathol (Berl) 1989, 78:410–418
46. Boellaard JW, Kao M, Schlote W, Diringer H: Neuronal autophagy in experimental scrapie. Acta Neuropathol (Berl) 1991, 82:225–228
47. Jeffrey M, Scott JR, Williams A, Fraser H: Ultrastructural features of spongiform encephalopathy transmitted to mice from three species of bovidae. Acta Neuropathol (Berl) 1992, 84:559–569
48. Baudhuin P, Hers HG, Loeb H: An electron microscopic and biochemical study of type II glycogenosis. Lab Invest 1964, 13:1139–1152
49. Novikoff AB: Lysosomes in nerve cells. The Neuron. Edited by Hyden H. Amsterdam, Elsevier Publishing Company, 1967, pp 319–377
50. Ivy GO: Protease inhibitors as a model for NCL disease, with special emphasis on the infantile and adult forms. Am J Med Genet 1992, 42:555–560
51. Suzuki T, Nakagawa M, Yoshikawa A, Sasagawa N, Yoshimori T, Ohsumi Y, Nishino I, Ishiura S, Nonaka I: The first molecular evidence that autophagy relates rimmed vacuole formation in chloroquine myopathy. J Biochem (Tokyo) 2002, 131:647–651
52. Komatsu M, Waguri S, Ueno T, Iwata J, Murata S, Tanida I, Ezaki J, Mizushima N, Ohsumi Y, Uchiyama Y, Kominami E, Tanaka K, Chiba T: Impairment of starvation-induced and constitutive autophagy in Atg7-deficient mice. J Cell Biol 2005, 169:425–434
53. Zhan SS, Beyreuther K, Schmitt HP: Neuronal ubiquitin and neurofilament expression in different lysosomal storage disorders. Clin Neuropathol 1992, 11:251–255
54. Ardley HC, Hung CC, Robinson PA: The aggravating role of the ubiquitin-proteasome system in neurodegeneration. FEBS Lett 2005, 579:571–576
55. Tanida I, Minematsu-Ikeguchi N, Ueno T, Kominami E: Lysosomal turnover, but not a cellular level, of endogenous LC3 is a marker for autophagy. Autophagy 2005, 1:84–91
56. Asanuma K, Tanida I, Shirato I, Ueno T, Takahara H, Nishitani T, Kominami E, Tomino Y: MAP-LC3, a promising autophagosomal marker, is processed during the differentiation and recovery of podocytes from PAN nephrosis. FASEB J 2003, 17:1165–1167
57. Hollenbeck PJ: Products of endocytosis and autophagy are retrieved from axons by regulated retrograde organelle transport. J Cell Biol 1993, 121:305–315
58. Larsen KE, Fon EA, Hastings TG, Edwards RH, Sulzer D: Methamphetamine-induced degeneration of dopaminergic neurons involves autophagy and upregulation of dopamine synthesis. J Neurosci 2002, 22:8951–8960
59. Lin WL, Lewis J, Yen SH, Hutton M, Dickson DW: Ultrastructural neuronal pathology in transgenic mice expressing mutant (P301L) human tau. J Neurocytol 2003, 32:1091–1105
60. Bednarski E, Ribak CE, Lynch G: Suppression of cathepsins B and L causes a proliferation of lysosomes and the formation of meganeurites in hippocampus. J Neurosci 1997, 17:4006–4021
61. Nixon RA, Wegiel J, Kumar A, Yu WH, Peterhoff C, Cataldo A, Cuervo AM: Extensive involvement of autophagy in Alzheimer disease: an immuno-electron microscopy study. J Neuropathol Exp Neurol 2005, 64:113–122
62. Mizushima N, Yamamoto A, Hatano M, Kobayashi Y, Kabeya Y, Suzuki K, Tokuhisa T, Ohsumi Y, Yoshimori T: Dissection of autophagosome formation using Apg5-deficient mouse embryonic stem cells. J Cell Biol 2001, 152:657–668
63. Eskelinen EL, Schmidt CK, Neu S, Willenborg M, Fuertes G, Salvador N, Tanaka Y, Lullmann-Rauch R, Hartmann D, Heeren J, von Figura K, Knecht E, Saftig P: Disturbed cholesterol traffic but normal proteolytic function in LAMP-1/LAMP-2 double-deficient fibroblasts. Mol Biol Cell 2004, 15:3132–3145

Available online at www.sciencedirect.com
SCIENCE DIRECT
Neuroscience Research 55 (2006) 28–33
Neuroscience Research
www.elsevier.com/locate/neures

Short-term potentiation at the parallel fiber–Purkinje cell synapse

Jun-Ichi Goto [a,b], Takafumi Inoue [a,c,*], Akinori Kuruma [a,b], Katsuhiko Mikoshiba [a,b,c]

[a] *Division of Molecular Neurobiology, The Institute of Medical Science, The University of Tokyo, 4-6-1 Shirokanedai, Minato-ku, Tokyo 108-8639 Japan*
[b] *Laboratory for Developmental Neurobiology, Brain Science Institute, RIKEN, 2-1 Hirosawa, Wako, Saitama 351-0198, Japan*
[c] *Calcium Oscillation Project, ICORP, Japan Science and Technology Corporation (JST), 3-14-4 Shirokanedai, Minato-ku, Tokyo 108-0071, Japan*

Received 6 January 2006; accepted 12 January 2006
Available online 10 February 2006

Abstract

Changes in synaptic efficacy at the parallel fiber (PF)–Purkinje cell (PC) synapse are postulated to be a cellular basis for motor learning. Although long-term efficacy changes lasting more than an hour at this synapse, i.e., long-term potentiation and depression, have been extensively studied, relatively short lasting synaptic efficacy changes, namely short-term potentiation (STP) lasting for tens of minutes, have not been discussed to date. Here we report that this synapse shows an apparent STP reliably by a periodic burst pattern of homosynaptic stimulation. This STP is presynaptically expressed, since it accompanies with a reduced paired-pulse facilitation and is resistant to postsynaptic Ca^{2+} reduction by BAPTA injection or in P/Q-type Ca channel knockout cerebella. This novel type of synaptic plasticity at the PF–PC synapse would be a clue for understanding the presynaptic mechanisms of plasticity at this synapse.

Keywords: Short-term potentiation; Purkinje cell; Parallel fiber; Synaptic plasticity; Electrophysiology; Cerebellum; Brain slice

1. Introduction

Plastic changes in synaptic efficacy are considered to be the cellular level of expression of the brain function, namely learning and memory. Long-term potentiation (LTP) of synaptic efficacy of excitatory synaptic potentials (EPSPs) at the Shaffer collateral and pyramidal cell synapse in the hippocampus CA1 area is one of the most extensively studied models for synaptic plasticity. In this synapse, potentiation induced by high frequency stimulation has been classified into three phases. Post-tetanic potentiation (PTP) is characterized by its shortest duration, terminating within seconds (Zucker and Regehr, 2002), which is followed by short-term potentiation (STP) lasting for 30-60 min. LTP follows STP, and lasts for hours to days. The nature of STP and the relationships between STP and LTP are still under debate. One hypothesis suggests that STP is a premature form of LTP in which LTP-induction stimulation was not enough to drive the plastic changes to a stable state (Gustafsson and Wigstrom, 1990; Hanse and Gustafsson, 1994). Another view is that the transient phase (STP) does not share cellular mechanisms with LTP (Schulz and Fitzgibbons, 1997; Volianskis and Jensen, 2003). The mechanistic nature and its role in synaptic encoding of STP in the CA1 pyramidal cell are unknown, which are awaited for the theories of memory retention and encoding (Albright et al., 2000).

The cerebellar cortex has been suggested to include an essential circuit for certain forms of motor learning, including associative eyeblink conditioning and adaptation of the vestibulo-ocular reflex. One cellular model system thought to contribute to learning in this structure is cerebellar long-term depression (LTD) in which coactivation of inferior olivary (climbing fiber) and granule cell (parallel fiber; PF) inputs to a Purkinje cell (PC) induces a persistent, input-specific depression of the PF–PC synapse (Ito, 2001). The converse phenomenon, cerebellar long-term potentiation (LTP), has also been described in which PF–PC synapses are strengthened by repetitive PF stimulation at low frequencies (Sakurai, 1987, 1990; Hirano, 1990, 1991; Crepel and Jaillard, 1991; Shibuki and Okada, 1992; Salin et al., 1996; Linden, 1997, 1998; Kimura et al., 1998; Storm et al., 1998; Linden and Ahn, 1999; Jacoby et al., 2001; Lev-Ram et al., 2002). In recent years, the molecular bases of cerebellar LTP have begun to be revealed. During sustained stimulation at 2–8 Hz, Ca^{2+} influx into

* Corresponding author. Tel.: +81 3 5449 5320; fax: +81 3 5449 5420.
E-mail address: tinoue@ims.u-tokyo.ac.jp (T. Inoue).

0168-0102/$ – see front matter © 2006 Elsevier Ireland Ltd and the Japan Neuroscience Society. All rights reserved.
doi:10.1016/j.neures.2006.01.001

presynaptic terminals activates PKA through activation of the Ca/calmodulin-sensitive adenylate cyclase and production of cAMP (Salin et al., 1996; Linden, 1997; Chavis et al., 1998; Linden and Ahn, 1999; Jacoby et al., 2001). An active zone protein RIM1α has been shown to be a potent target of PKA for LTP induction at this synapse (Castillo et al., 2002; Lonart et al., 2003). Besides this presynaptic LTP, Lev-Ram et al. (2002) reported a postsynaptic form of LTP, which depends on nitric oxide, induced by 1 Hz PF stimulation at the PF–PC synapse.

Compared with the rather accumulated knowledge about the molecular basis of LTP at the PF–PC synapse, nothing has been discussed so far about potentiation of synaptic efficacy lasting a middle range of period, i.e., tens of minutes, like STP at the CA3–CA1 synapse. Here we report that PF–PC synapse shows STP which lasts 20–30 min reliably by a periodic burst pattern (five shocks at 50 Hz at a frequency of 1 Hz for 90 s). This form of synaptic plasticity would be a clue for understanding the presynaptic mechanisms of plasticity at this synapse.

2. Materials and methods

2.1. Preparation of cerebellar slices

Parasagittal cerebellar slices were prepared from 14–17 days old C57BL/6J mice (CLEA Japan Inc., Japan) or homozygous P/Q-type Ca channel (α_{1A} subunit) knock out mice (F7–F9 hybrid of 129 and C57BL/6J lines; Kulik et al., 2004) of either sex. Standard techniques were used to prepare 250 μm thick parasagittal cerebellar slices (Kuruma et al., 2003) using a vibratome-type tissue slicer (Leica Microsystems, Germany). Slices were incubated for 30 min at 37 °C and then kept at room temperature until recording, in the artificial cerebro-spinal fluid (ACSF) containing (in mM) 124 NaCl, 2.5 KCl, 2 $CaCl_2$, 2 $MgCl_2$, 1.25 NaH_2PO_4, 20 D-glucose, 26 $NaHCO_3$ and saturated with 95% O_2 and 5% CO_2. All experimental procedures were performed in accordance with the instructions of the Institute of Medical Science, The University of Tokyo for animal care and use.

2.2. Electrophysiology

Slices were transferred to recording chamber and continuously superfused with ACSF containing 10 μM bicuculline methochloride (Tocris, UK) at 2.5 ml/min, 30–32 °C. Visually guided patch clamp methods are described previously (Kuruma et al., 2003). Patch pipettes were pulled with an open tip resistance of 3–6 MΩ when filled with an internal pipette solution containing (in mM) 140 K-gluconate, 10 Hepes, 4 NaCl, 4 MgATP, 0.3 NaGTP, 0.2 bis-fura-2, and pH was adjusted to 7.3. For the experiment of intracellular infusion of BAPTA, 20 mM BAPTA (Sigma–Aldrich Co., USA) was added to the pipette solution prior to the pH adjustment. Osmolarity of internal solutions was adjusted between 280 and 290 mOsm.

Tightly sealed patch membrane was ruptured and the membrane potentials were recorded in current clamp mode using an Axoclamp 2B amplifier (Molecular Devices Corp., USA). Membrane potentials were kept at −65 mV by injecting negative currents. Experiments were rejected if the holding current exceeded −650 pA, or the junction potential drift was greater than ±5 mV, or the access resistance exceeded 25 MΩ. Input resistances were 120 MΩ to more than 1 GΩ. Initial access resistances were varied among 10–20 MΩ, and continuously compensated during recording periods. PF–PC synaptic responses were evoked with a glass electrode with an open tip of 1–3 μm, filled with ACSF, placed on the surface of the distal part of molecular layer of slices.

Excitatory postsynaptic potentials (EPSPs) were evoked at 0.2 Hz by constant-current pulses of 5–20 μA for 200 μs. Prior to each PF stimulus, a hyperpolarizing current pulse was injected through the patch pipette to monitor the series and input resistances and also to prevent cell firing, and the peak amplitude of EPSP was compensated by fitting hyperpolarizing Vm curve with a single exponential function.

After a stable baseline recording of EPSPs (4–10 mV in amplitudes), STP was induced by 90 trains of five shocks at 50 Hz at a frequency of 1 Hz. During the STP inducing stimuli were applied, membrane current was recorded in the voltage clamp mode at −60 mV and simultaneous Ca^{2+} imaging was performed. In BAPTA infusion experiments, STP was induced more than 15 min after whole-cell rupture. Cells with unstable baseline recording (>±5% deviation of the normalized EPSP in any of each 2 min recording during a 6 min baseline period in PPF and BAPTA experiments and during 10 min in other experiments) were excluded from the analysis.

2.3. Paired-pulse facilitation

Paired-pulse facilitation was measured before and after the STP induction: just prior to STP induction and at 5, 10, 15 and 20 min after the STP induction.

Each PPF test consisted of five trains of paired pulse of 80 ms interval separated by 5 s. EPSC was used as an index of synaptic strength in the PPF experiment, because measuring synaptic strength as EPSC in voltage-clamp mode has the merit to suppress voltage-activated currents which would bias especially the amplitude of facilitated second synaptic response to a pair of stimuli. However, we preferred the EPSP amplitude as an index for the long-term changes in synaptic efficacy, because EPSC amplitude is more sensitive to changes in the series resistance.

2.4. Fluorescence imaging of calcium concentration

Cytosolic Ca^{2+} concentration changes were measured by fluorescence changes of bis-fura-2 loaded through patch pipettes. Detailed methods were described previously (Kuruma et al., 2003) with a difference in a CCD camera type. An ORCA ER (Hamamatsu Photonics, Japan) was used as a detector. Ca^{2+} imaging was performed only during the STP-induction stimulation. Bis-fura-2 was loaded from the cell body for at least 20 min, and after stable baseline of EPSP was recorded, focus of microscope was adjusted on a part of dendrite close to the tip of stimulating electrode by means of bis-fura-2 fluorescence. Soon after, the STP-inducing stimuli were applied. A set of three consecutive image stacks each of which covers each Ca^{2+} transient evoked by a train of 50 Hz stimuli was taken every 29 s, and the total 12 fluorescence image stacks were used to create an averaged image to improve S/N ratio, and rectangular regions of interest (ROIs) of proper size were placed on the dendritic area. Fluorescence intensities (F) included in each ROI were averaged to represent fluorescence signal of the ROI. Ca^{2+} signals were represented by $\Delta F/F_0$, where F_0 is F of the first frame and ΔF is $F - F_0$, to normalize uneven distribution of chromophore. ROI positions were determined as to maximize the Ca^{2+} transient. When amplitude of evoked Ca^{2+} transient was smaller than 3 × S.D. of the baseline signal, the record was omitted from the analysis.

2.5. Data analysis

Electrophysiological and Ca^{2+} imaging data were acquired and analyzed using custom software TI workbench (written by T.I.).

All the data are expressed as mean ± S.E.M.

3. Results

We examined the effect of periodic burst stimuli at the PF–PC synapse in acute mouse cerebellar slice. Ninety trains of periodic bursts, which consist of five pulses at 50 Hz PF stimuli, at a frequency of 1 Hz resulted in a robust potentiation in synaptic efficacy which lasted for 10–20 min (Fig. 1). EPSP amplitudes were increased to 139.4 ± 5.6% of baseline 5 min after the burst stimulation (Fig. 1B, $n = 12$), which gradually decayed and returned to the baseline level after 20 min. This

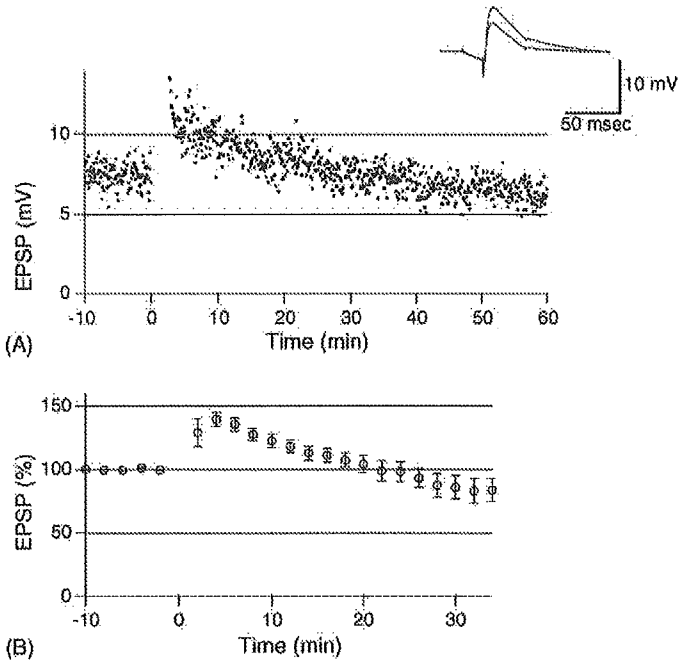

Fig. 1. Periodic burst stimuli induced STP at the PF–PC synapse which lasted 20–30 min. PF burst stimuli were applied after 10 min of stable baseline recording, and changes in EPSP amplitude were recorded thereafter. Monitoring EPSP amplitudes was done at 0.2 Hz throughout the recordings. (A) A representative trace of STP. Inset shows two overlaid EPSP traces before and 5 min after the STP induction each of which is an average trace of consecutive 24 traces (2 min). Apparent potentiation in EPSP amplitude is shown, while preceding overlapping hyperpolarizations induced by constant negative current injections indicate no apparent change in the postsynaptic membrane conductance. (B) Averaged result. Each data point shows mean normalized EPSP amplitude ± S.E.M. of consecutive 2 min records ($n = 12$).

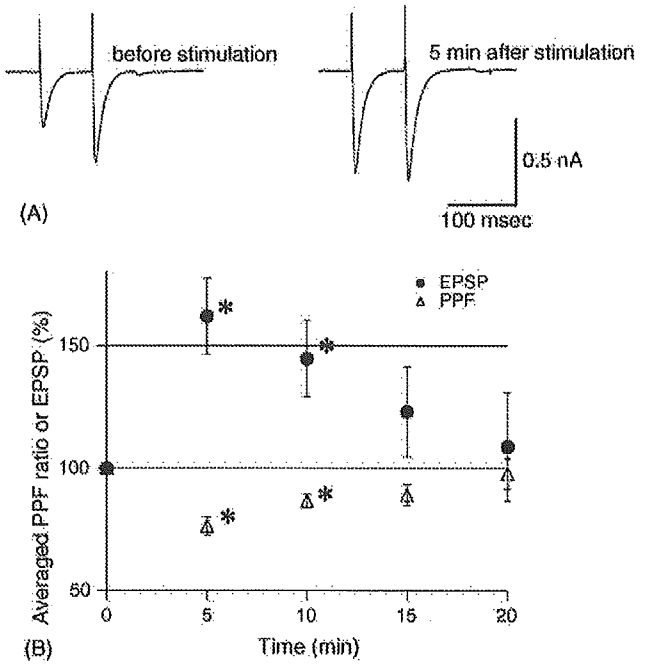

Fig. 2. Paired pulse ratio decreased in accordance with EPSP potentiation, and gradually recovered in parallel with the decay of STP. (A) Representative traces of EPSCs in response to a pair of PF stimuli separated by 80 ms recorded before and 5 min after PF short burst stimulation. (B) Time course of EPSP amplitude and paired pulse ratio. Paired pulse ratio decreased after STP induction and gradually returned to the baseline level by 20 min. This time course was almost in parallel with that of change in EPSP. $^{*}P < 0.01$, compared with the value at time zero (just before STP induction), paired t-test, $n = 5$.

periodic burst stimulation is similar to the stimulation protocol used for LTD induction at PF–PC synapse in rat cerebellar slices (Eilers et al., 1997), however, we detected only slight depression (~90% of baseline on average) at 30 min after the periodic burst stimulation.

To distinguish whether the observed STP is expressed at pre- or postsynapse, we measured paired-pulse facilitation (PPF) before and after the short burst stimuli. Paired-pulse facilitation is associated with a residual Ca^{2+} transient in the PF terminal after the first action potential (Atluri and Regehr, 1998) and an increase in transmitter release (Zucker and Regehr, 2002). Changes in the paired pulse ratio of the second pulse to the first can be affected by known modulators of transmitter release and are generally taken to reflect changes in the release probability (Dittman and Regehr, 1996). Paired pulse ratio was significantly decreased after the burst stimuli (Fig. 2, $P < 0.01$ at 5 and 10 min after stimuli, compared with the paired pulse ratio taken just before the burst stimuli, paired t-test, $n = 5$). Paired pulse ratio returned to the baseline level 20 min after the burst stimuli in parallel with the decay of the increased amplitude of EPSPs. These results suggest that presynaptic mechanisms, which affect the paired pulse ratio, underlie the observed STP at least to some extent.

Next we examined the contribution of Ca^{2+} dependent mechanism to the generation of STP. In hippocampal CA3–CA1 synapses, STP requires *N*-methyl-D-aspartate (NMDA) receptor mediated postsynaptic Ca^{2+} elevation (Malenka and Nicoll, 1993). As PCs do not express functional NMDA receptors (Konnerth et al., 1990; Perkel et al., 1990; Farrant and Cull-Candy, 1991), voltage-gated Ca channels may play a pivotal role for regulation of cytoplasmic Ca^{2+} dynamics in PC dendrites (Kuruma et al., 2003; Hartmann and Konnerth, 2005). To investigate the involvement of Ca^{2+} signals in the induction of STP, we tested the effect of ablation of P/Q-type Ca channel, which is the major subtype of voltage-gated Ca channel expressed in PC (Usowicz et al., 1992). PF–PC synapses of mouse with disrupted α1A genes, encoding a pore-forming subunit of P/Q-type Ca channel, showed almost the same time course of STP induction and decay over 10–20 min (Fig. 3A). During the STP induction period, amplitudes of Ca^{2+} transients evoked by each PF burst were measured in PC dendrites (see Section 2). Since severe reduction in Ca^{2+} transient evoked by the STP inducing stimuli was detected in knockout PC dendrites ($8.3 \pm 1.2\%$ in wild type and $3.8 \pm 0.5\%$ in $\Delta F/F$ in mutants, $P < 0.05$, Mann–Whitney test, $n = 9$ and 3, respectively), it may be less plausible that the postsynaptic Ca^{2+} changes play a major role in the STP expression.

To further examine whether the postsynaptic Ca^{2+} take a part in the expression of STP, we inhibited postsynaptic Ca^{2+} changes by loading Ca^{2+} chelator BAPTA (20 mM) through patch pipettes, which condition totally blocks postsynaptically expressed LTD at the PF–PC synapse (Konnerth et al., 1992;

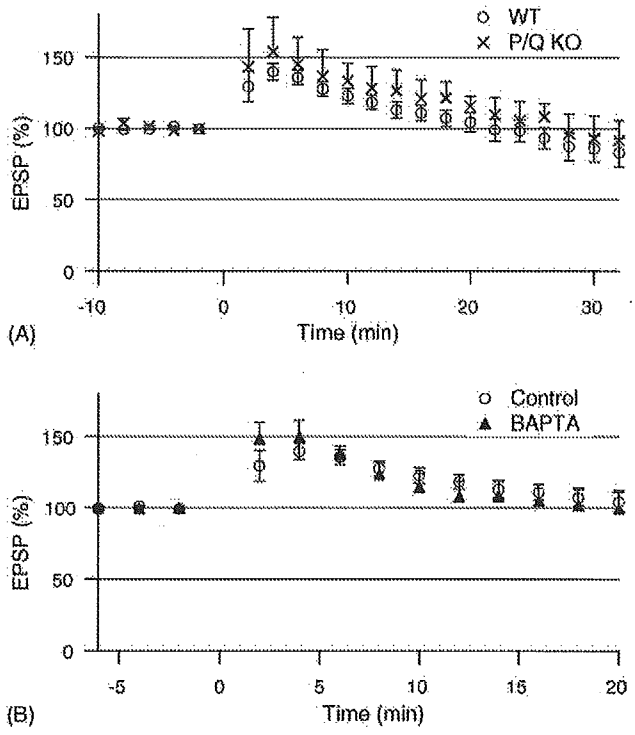

Fig. 3. Inhibition of postsynaptic Ca^{2+} did not affect the amplitude and time course of STP. (A) P/Q-type Ca channel knockout mouse. The PF–PC synapse of P/Q-type Ca channel knock out mice ($n = 3$) showed similar time course and amplitude of EPSP changes as those of wild type ($n = 12$, same trace as shown in Fig. 1B). (B) Postsynaptic BAPTA infusion. Postsynaptic BAPTA infusion (20 mM; $n = 5$) had no obvious effect on the amplitude and overall time course of STP. Averaged STP time course of wild type is overlaid ($n = 12$, same data set as shown in Fig. 1B).

Reynolds and Hartell, 2000) while presynaptically expressed LTP unaffected (Salin et al., 1996). After STP inducing short burst PF stimulation, EPSP amplitude was increased by 149 ± 12% of baseline and gradually decayed in a time course similar to that of control experiments (Fig. 3B). This result further suggests that STP is independent of postsynaptic Ca^{2+} dependent mechanisms. All the results suggest that STP induced by the short burst stimuli at PF–PC synapse is expressed presynaptically.

4. Discussion

We have shown here that repeated burst stimuli at the PF–PC synapse result in potentiation in synaptic efficacy lasting for 20–30 min. Such "short-term potentiation" of a range of 10–30 min has been well characterized at the Schaffer collaterals and pyramidal cell synapse in the hippocampus CA1 area, where STP is phenomenologically isolated from much shorter PTP of second-long (Zucker and Regehr, 2002) and from much longer LTP which lasts more than hours (Volianskis and Jensen, 2003). STP has been related to an early phase of LTP (Gustafsson and Wigstrom, 1990; Malenka, 1991; Colino et al., 1992; Hanse and Gustafsson, 1994; Xie et al., 1996), or STP and LTP have been considered as reflections of two distinct phenomena (Kauer et al., 1988; Schulz and Fitzgibbons, 1997; Volianskis and Jensen, 2003). The mechanistic nature and its role of STP in the hippocampus CA1 area are thus still under debate.

The mossy fiber–pyramidal cell synapse in the hippocampus CA3 region is also extensively studied for LTP, however, existence of STP-like synaptic efficacy change has been rarely discussed in this synapse. Exceptionally, mossy fiber synapse from mice lacking genes encoding Rab3A (Castillo et al., 1997) or RIM1α (Castillo et al., 2002) lacks LTP and potentiated synaptic efficacy returns to the basal level within 10–20 min. The PF–PC synapse shares some features with the mossy fiber–pyramidal cell synapse. Both synapses show presynaptically expressed PKA-dependent LTP (Nicoll and Malenka, 1995; Salin et al., 1996; Linden, 1997; Chavis et al., 1998; Linden and Ahn, 1999; Jacoby et al., 2001). And further, the PF–PC LTP also depends on RIM1α, as it returns to the baseline within 10–20 min in RIM1α knockout mice (Castillo et al., 2002). Without this exception, there has been no report about STP-like synaptic potentiation which decays over 20–30 min in the PF–PC synapse. If STP revealed in this study share molecular mechanisms with the LTP induction in this synapse, the STP induction protocol employed in this study might be a clue to dissect the molecular mechanisms of early steps of LTP induction at PF–PC synapse. Or it would be also interesting if STP found in this study is a distinct phenomenon from LTP.

We revealed that STP found in this study is presynaptically expressed according to the following observations. Firstly, STP was accompanied by a decrease in paired pulse ratio with a similar recovery time course (Fig. 2B). Changes in the paired pulse ratio of the second pulse to the first are generally taken to reflect changes in the release probability (Dittman and Regehr, 1996). Secondly, STP was not affected by postsynaptic BAPTA loading which blocks postsynaptic Ca^{2+} dependent events (Fig. 3B). Finally STP was similarly observed in P/Q-type Ca channel knockout mice (Fig. 3A), in which amplitudes of postsynaptic Ca^{2+} transients evoked by the STP-inducing stimulation were apparently reduced (see Section 3). Whether or not this STP and presynaptically expressed LTP are reflections of a single process of potentiation that includes multiple phases or whether this STP and the LTP are distinct phenomena remained to be elucidated.

Eilers et al. (1997) reported a homosynaptic LTD at the PF–PC synapse by a similar stimulation pattern as used in this study. Two to five pulses at 10–50 Hz at a frequency of 1 Hz for 1–2 min resulted in a robust depression of PF synaptic responses (58%). We did not observe such a robust long-lasting depression of PF responses in this study (~90% of baseline 30 min after the induction) with five pulses at 50 Hz at a frequency of 1 Hz for 1.5 min, but did observe STP. Differences in the experimental conditions may explain the different results: mouse was used in this study and rat in the other, and the bath temperature was 30–32 °C in this study and 20–22 °C in the other. Nevertheless, we do not consider that the STP observed in this study is simply an overlap of postsynaptic LTD and presynaptic LTP, because STP was not affected by postsynaptic loading of BAPTA (Fig. 3B) and the time course of paired pulse ratio change was in accordance with that of synaptic efficacy change (Fig. 2B).

The stimulation pattern for induction of STP employed in this study was different from the LTP-inducing stimulation patterns employed in recent studies in that the former is composed of periodic burst of 50 Hz trains and the latter uses evenly spaced pulses at 2–8 Hz (Salin et al., 1996; Linden, 1997; Chavis et al., 1998; Linden and Ahn, 1999; Jacoby et al., 2001). Although the averaged numbers of stimuli of the both stimulations fall in the same range (5 times/s versus 2–8 Hz), bursting action potentials at the PF terminal might result in much higher accumulation of Ca^{2+} in presynapse which would result in a different consequence, i.e., STP, from the slow and evenly spaced arrival of action potentials. Since the firing frequency of cerebellar granule cells is around 10–50 Hz at resting and increased by 50–100 Hz under sensory stimulations recorded in vivo (Ito, 2001; Chadderton et al., 2004), the periodic bursting PF stimuli employed in this study may represent a physiologically occurring firing pattern.

Acknowledgements

We thank Dr. Chihiro Hisatsune for discussions and Mr. Akira Futatsugi and Mses. Etsuko Ebisui and Mizuki Yamada for breeding the mutant mice.

References

Albright, T.D., Jessell, T.M., Kandel, E.R., Posner, M.I., 2000. Neural science: a century of progress and the mysteries that remain. Cell 100 (Suppl.), S1–S55.

Atluri, P.P., Regehr, W.G., 1998. Delayed release of neurotransmitter from cerebellar granule cells. J. Neurosci. 18, 8214–8227.

Castillo, P.E., Janz, R., Sudhof, T.C., Tzounopoulos, T., Malenka, R.C., Nicoll, R.A., 1997. Rab3A is essential for mossy fibre long-term potentiation in the hippocampus. Nature 388, 590–593.

Castillo, P.E., Schoch, S., Schmitz, E., Sudhof, T.C., Malenka, R.C., 2002. RIM1α is required for presynaptic long-term potentiation. Nature 415, 327–330.

Chadderton, P., Margrie, T.W., Hausser, M., 2004. Integration of quanta in cerebellar granule cells during sensory processing. Nature 428, 856–860.

Chavis, P., Mollard, P., Bockaert, J., Manzoni, O., 1998. Visualization of cyclic AMP-regulated presynaptic activity at cerebellar granule cells. Neuron 20, 773–781.

Colino, A., Huang, Y.Y., Malenka, R.C., 1992. Characterization of the integration time for the stabilization of long-term potentiation in area CA1 of the hippocampus. J. Neurosci. 12, 180–187.

Crepel, R., Jaillard, D., 1991. Pairing of pre- and postsynaptic activities in cerebellar Purkinje cells induces long-term changes in synaptic efficacy in vitro. J. Physiol. 432, 123–141.

Dittman, J.S., Regehr, W.G., 1996. Contributions of calcium-dependent and calcium-independent mechanisms to presynaptic inhibition at a cerebellar synapse. J. Neurosci. 16, 1623–1633.

Eilers, J., Takechi, H., Finch, E.A., Augustine, G.J., Konnerth, A., 1997. Local dendritic Ca^{2+} signaling induces cerebellar long-term depression. Learn. Mem. 4, 159–168.

Farrant, M., Cull-Candy, S.G., 1991. Excitatory amino acid receptor-channels in Purkinje cells in thin cerebellar slices. Proc. Biol. Sci. 244, 179–184.

Gustafsson, B., Wigstrom, H., 1990. Long-term potentiation in the hippocampal CA1 region: its induction and early temporal development. Prog. Brain. Res. 83, 223–232.

Hanse, E., Gustafsson, B., 1994. Onset and stabilization of NMDA receptor-dependent hippocampal long-term potentiation. Neurosci. Res. 20, 15–25.

Hartmann, J., Konnerth, A., 2005. Determinants of postsynaptic Ca^{2+} signaling in Purkinje neurons. Cell Calcium 37, 459–466.

Hirano, T., 1990. Depression and potentiation of the synaptic transmission between a granule cell and a Purkinje cell in rat cerebellar culture. Neurosci. Lett. 119, 141–144.

Hirano, T., 1991. Synaptic formations and modulations of synaptic transmissions between identified cerebellar neurons in culture. J. Physiol. (Paris) 85, 145–153.

Ito, M., 2001. Cerebellar long-term depression: characterization, signal transduction, and functional roles. Physiol. Rev. 81, 1143–1195.

Jacoby, S., Sims, R.E., Hartell, N.A., 2001. Nitric oxide is required for the induction and heterosynaptic spread of long-term potentiation in rat cerebellar slices. J. Physiol. 535, 825–839.

Kauer, J.A., Malenka, R.C., Nicoll, R.A., 1988. NMDA application potentiates synaptic transmission in the hippocampus. Nature 334, 250–252.

Kimura, S., Uchiyama, S., Takahashi, H.E., Shibuki, K., 1998. cAMP-dependent long-term potentiation of nitric oxide release from cerebellar parallel fibers in rats. J. Neurosci. 18, 8551–8558.

Konnerth, A., Llano, I., Armstrong, C.M., 1990. Synaptic currents in cerebellar Purkinje cells. Proc. Natl. Acad. Sci. U.S.A. 87, 2662–2665.

Konnerth, A., Dreessen, J., Augustine, G.J., 1992. Brief dendritic calcium signals initiate long-lasting synaptic depression in cerebellar Purkinje cells. Proc. Natl. Acad. Sci. U.S.A. 89, 7051–7055.

Kulik, A., Nakadate, K., Hagiwara, A., Fukazawa, Y., Lujan, R., Saito, H., Suzuki, N., Futatsugi, A., Mikoshiba, K., Frotscher, M., Shigemoto, R., 2004. Immunocytochemical localization of the α1A subunit of the P/Q-type calcium channel in the rat cerebellum. Eur. J. Neurosci. 19, 2169–2178.

Kuruma, A., Inoue, T., Mikoshiba, K., 2003. Dynamics of Ca^{2+} and Na^{+} in the dendrites of mouse cerebellar Purkinje cells evoked by parallel fibre stimulation. Eur. J. Neurosci. 18, 2677–2689.

Lev-Ram, V., Wong, S.T., Storm, D.R., Tsien, R.Y., 2002. A new form of cerebellar long-term potentiation is postsynaptic and depends on nitric oxide but not cAMP. Proc. Natl. Acad. Sci. U.S.A. 99, 8389–8393.

Linden, D.J., 1997. Long-term potentiation of glial synaptic currents in cerebellar culture. Neuron 18, 983–994.

Linden, D.J., 1998. Synaptically evoked glutamate transport currents may be used to detect the expression of long-term potentiation in cerebellar culture. J. Neurophysiol. 79, 3151–3156.

Linden, D.J., Ahn, S., 1999. Activation of presynaptic cAMP-dependent protein kinase is required for induction of cerebellar long-term potentiation. J. Neurosci. 19, 10221–10227.

Lonart, G., Schoch, S., Kaeser, P.S., Larkin, C.J., Sudhof, T.C., Linden, D.J., 2003. Phosphorylation of RIM1α by PKA triggers presynaptic long-term potentiation at cerebellar parallel fiber synapses. Cell 115, 49–60.

Malenka, R.C., 1991. Postsynaptic factors control the duration of synaptic enhancement in area CA1 of the hippocampus. Neuron 6, 53–60.

Malenka, R.C., Nicoll, R.A., 1993. NMDA-receptor-dependent synaptic plasticity: multiple forms and mechanisms. Trends Neurosci. 16, 521–527.

Nicoll, R.A., Malenka, R.C., 1995. Contrasting properties of two forms of long-term potentiation in the hippocampus. Nature 377, 115–118.

Perkel, D.J., Hestrin, S., Sah, P., Nicoll, R.A., 1990. Excitatory synaptic currents in Purkinje cells. Proc. Biol. Sci. 241, 116–121.

Reynolds, T., Hartell, N.A., 2000. An evaluation of the synapse specificity of long-term depression induced in rat cerebellar slices. J. Physiol. 527 (Pt 3), 563–577.

Sakurai, M., 1987. Synaptic modification of parallel fibre–Purkinje cell transmission in in vitro guinea-pig cerebellar slices. J. Physiol. 394, 463–480.

Sakurai, M., 1990. Calcium is an intracellular mediator of the climbing fiber in induction of cerebellar long-term depression. Proc. Natl. Acad. Sci. U.S.A. 87, 3383–3385.

Salin, P.A., Malenka, R.C., Nicoll, R.A., 1996. Cyclic AMP mediates a presynaptic form of LTP at cerebellar parallel fiber synapses. Neuron 16, 797–803.

Schulz, P.E., Fitzgibbons, J.C., 1997. Differing mechanisms of expression for short-and long-term potentiation. J. Neurophysiol. 78, 321–334.

Shibuki, K., Okada, D., 1992. Cerebellar long-term potentiation under suppressed postsynaptic Ca^{2+} activity. Neuroreport 3, 231–234.

Storm, D.R., Hansel, C., Hacker, B., Parent, A., Linden, D.J., 1998. Impaired cerebellar long-term potentiation in type I adenylyl cyclase mutant mice. Neuron 20, 1199–1210.

Usowicz, M.M., Sugimori, M., Cherksey, B., Llinas, R., 1992. P-type calcium channels in the somata and dendrites of adult cerebellar Purkinje cells. Neuron 9, 1185–1199.

Volianskis, A., Jensen, M.S., 2003. Transient and sustained types of long-term potentiation in the CA1 area of the rat hippocampus. J. Physiol. 550, 459–492.

Xie, X., Barrionuevo, G., Berger, T.W., 1996. Differential expression of short-term potentiation by AMPA and NMDA receptors in dentate gyrus. Learn. Mem. 3, 115–123.

Zucker, R.S., Regehr, W.G., 2002. Short-term synaptic plasticity. Annu. Rev. Physiol. 64, 355–405.

Development/Plasticity/Repair

ORP150/HSP12A Regulates Purkinje Cell Survival: A Role for Endoplasmic Reticulum Stress in Cerebellar Development

Yasuko Kitao,[1] Kouichi Hashimoto,[2] Tomohiro Matsuyama,[4] Hiroyuki Iso,[5] Takeshi Tamatani,[1] Osamu Hori,[1,3] David M. Stern,[6] Masanobu Kano,[2] Kentaro Ozawa,[1] and Satoshi Ogawa[1,3]

Departments of [1]Neuroanatomy and [2]Cellular Neurophysiology, Graduate School of Medical Science, Kanazawa University, Kanazawa 920-8640, Japan, [3]Core Research for Evolutional Science and Technology, Japan Science and Technology, Kawaguchi 332-0012, Japan, Departments of [4]Internal Medicine and [5]Behavior Science, Hyogo College of Medicine, Nishinomiya 663-8501, Hyogo, Japan, and [6]Dean's Office, Medical College of Georgia, Augusta, Georgia 30912

The endoplasmic reticulum (ER) stress response contributes to neuronal survival in ischemia and neurodegenerative processes. ORP150 (oxygen-regulated protein 150)/HSP12A (heat shock protein 12A), a novel stress protein located in the ER, was markedly induced in Purkinje cells maximally at 4–8 d after birth, a developmental period corresponding to their vulnerability to cell death. Both terminal deoxynucleotidyl transferase-mediated biotinylated UTP nick end-labeling analysis and immunostaining using anti-activated caspase-3 antibody revealed that transgenic mice with targeted neuronal overexpression of ORP150 (Tg ORP150) displayed diminished cell death in the Purkinje cell layer and increased numbers of Purkinje cells up to 40 d after birth ($p < 0.01$), compared with those observed in heterozygous ORP150/HSP12A-deficient (ORP150 $^{+/-}$) mice and wild-type littermates (ORP150 $^{+/+}$). Cultured Purkinje cells from Tg ORP150 mice displayed resistance to both hypoxia- and AMPA-induced stress. Behavioral analysis, using rotor rod tasks, indicated impairment of cerebellar function in Tg ORP150 animals, consistent with the concept that enhanced survival of Purkinje cells results in dysfunction. These data suggest that ER chaperones have a pivotal role in Purkinje cell survival and death and thus may highlight the importance of ER stress in neuronal development.

Key words: **apoptosis; [Ca]; cerebellum; death; Purkinje cell; glutamate; neuronal cell death; calbindin; cerebellar ataxia**

Introduction

Among cells constituting the CNS, neurons are especially vulnerable to fluctuations in the extracellular environment, including ischemic stress, trauma, and a range of infectious challenges. Moreover, within the general population of neurons, certain subsets display enhanced vulnerability to particular toxic insults. One mechanism often invoked to explain neuronal susceptibility to stress is their response to glutamate (Coyle and Puttfarchen, 1993). For example, in ischemia, glutamate toxicity is likely to exacerbate neuronal death, along with hypoxia, glucose deprivation, and the generation of reactive oxygen intermediates (Siesjoe, 1988). Glutamate–receptor interaction ultimately triggers elevation of intracellular [Ca^{2+}] ([Ca^{2+}]i), the final common pathway of cell death attributable, at least in part, to activation of intracellular Ca^{2+}-dependent proteinases, such as calpain/cathepsin, caspases, and p35 (Lee et al., 2000). Thus, cellular mechanisms that buffer these events could have a protective role, potentially early in the ischemic process.

In contrast, astrocytes are considerably more resistant to environmental challenge. On the basis of this phenotypic difference in cell behavior, we have cloned a stress protein induced by oxygen deprivation, ORP150 (oxygen-regulated protein 150), and have shown it to have a central role in cellular survival in hypoxia (Kuwabara et al., 1996; Ozawa et al., 1999). Subsequently, we analyzed neuronal expression of ORP150 and found that it contributes to maintenance of cell viability in ischemia, although the time course and level of ORP150 expression were quite different than in astrocytes (Tamatani et al., 2001). In hippocampal neuronal cultures, ORP150 induced in the endoplasmic reticulum (ER) in response to hypoxia stabilized [Ca^{2+}]i, thereby suppressing activation of Ca^{2+}-dependent proteinases (Kitao et al., 2001). Furthermore, adenovirus-mediated expression of ORP150 in the hippocampus suppressed, at least partly, delayed neuronal cell death (Miyazaki et al., 2002). These data suggest a central role for the ER-associated molecular chaperone ORP150 in the defense of neurons to environmental stress.

Cerebellar Purkinje cells represent a group of neurons highly vulnerable to ischemic and excitotoxic stress (Welsh et al., 2002). The effect of ischemic stress on Purkinje cells has been difficult to analyze *in vivo* because of methodological difficulties, especially in mice (Hata et al., 1993; Sieber et al., 1995). However, it has become clear that ischemia-related stress responses are operative during brain development, suggesting an overlap of basic cellular properties marshaled to deal with physiological and pathological environmental conditions (Calabrese et al., 2002). Therefore, a

Received Sept. 2, 2003; revised Dec. 15, 2003; accepted Dec. 15, 2003.

We thank F. Ichinoda (Department of Neuroanatomy, Kanazawa University Medical School) and K. Obata (Department of Internal Medicine, Hyogo College of Medicine) for expert technical support.

Correspondence should be addressed to Dr. Yasuko Kitao, Department of Neuroanatomy, Kanazawa University Medical School, 13-1 Takara-machi, Kanazawa City 920-8640, Ishikawa, Japan. E-mail: kitao@nanat.m.kanazawa-u.ac.jp.

DOI:10.1523/JNEUROSCI.4029-03.2004

 0270-6474/04/241486-11$15.00/0

strategy contributing to Purkinje cell survival in development might also lead to recognition of protective mechanisms relevant to pathophysiological situations.

In this report, we demonstrate that expression of ORP150 in the cerebellum occurs especially in Purkinje cells early after birth. Purkinje cell death observed in this developmental period was correlated with induction of ORP150, potentially representing incomplete protection attributable to insufficient endogenous expression of ORP150, compared with other cell types, such as astrocytes (Tamatani et al., 2001). Consistent with this concept, transgenic (Tg) mice with targeted neuronal overexpression of ORP150 displayed decreased Purkinje cell death and increased numbers of Purkinje cells in the cerebellum (with associated changes in cerebellar function), whereas the opposite was observed in mice heterozygous for deletion of the ORP150 gene ($ORP150^{+/-}$; note that $ORP150^{-/-}$ mice display an embryonic lethal phenotype). These data suggest the role of ER stress, through induction of ORP150, and, potentially, other factors in modulating Purkinje cell vulnerability during development and postnatally in stress responses.

Materials and Methods

Animals. Mice deficient in ORP150 were originally generated by Kitao et al. (2001). Germ line transmission of the mutationally inactivated ORP150 gene was achieved, and mice were backcrossed into the C57BL/6 strain (N10). Genotype assignment of offspring was determined by Southern blotting of genomic DNA from tails. Transgenic mice with targeted neuronal expression of wild-type ORP150 were made using the platelet-derived growth factor (PDGF) B-chain promoter (Sasahara et al., 1991). The latter animals were made and characterized as described (Tamatani et al., 2001). Offspring that carried the transgene were identified by Southern blotting and bred into the C57BL/6 strain (N10).

Histochemistry. Animals were perfused with paraformaldehyde (4%) under deep anesthesia, and brains were cut into parasagittal slices on a cryostat. Sections were processed for cresyl violet staining or for immunohistochemistry using anti-rabbit human ORP150 IgG (5 μg/ml; Kuwabara et al., 1996; Kitao et al., 2001; Ozawa et al., 2001), monoclonal mouse anti-calbindin D_{28K} IgG (Sigma, St. Louis, MO; 1:1000 dilution), mouse anti-growth arrest- and DNA damage-inducible gene 153/CHOP (C/EBP-homologous protein) IgG (Santa Cruz Biotechnology, Santa Cruz, CA; 1:100 dilution), mouse anti-Lys-Asp-Glu-Leu (KDEL) IgG (Stressgen Biotechnologies Co. ; 1:500 dilution), rabbit anti-HSP72 (72 kDa heat shock protein) IgG (Stressgen Biotechnologies Co. ; 1:500 dilution), or mouse anti-activated JNK1 (Jun kinase 1) IgG (Sigma; 1:100 dilution). The density and size of Purkinje cells were calculated as described previously (Baader et al., 1998). In brief, every 10th section (10 μm thickness) was evaluated by counting the number of Purkinje cells. The mean Purkinje cell (PC) number per section was derived from five sections. For area measurements, every third section (40 μm thickness) was measured in a digital captured image using Photoshop software (Adobe Systems, Tokyo, Japan). The cell density and size were also measured in the granular cell layer according to the protocol by Kakizawa et al. (2000). In brief, mice were perfusion-fixed at 30 d after birth. After the staining of a sagittal section (10 μm thickness) with cresyl violet, granular cell density in lobules 4 and 5 was counted. In each case, two observers without knowledge of the experimental protocol evaluated sections, and experiments were repeated at least three times.

Assessment of neuronal cell death in vivo. Parasagittal cerebellar sections were evaluated by terminal deoxynucleotidyl transferase-mediated biotinylated UTP nick end-labeling (TUNEL) staining (Trevigen Apoptotic Cell System 2 terminal deoxynucleotidyl transferase-fluor *in situ* apoptosis detection kit; Trevigen, Inc.) and immunostaining with antibody to activated caspase-3 (Genzyme, Boston, MA; 0.3 μg/ml final concentration). Calbindin D_{28K}-positive neurons were identified as Purkinje cells and counted in sections in three fields (magnification, 40×; Han et al., 2001). Purkinje cells staining positively by either the TUNEL method or with anti-activated caspase-3 antibody were scored as dead cells. Neurons in the other parts of the brain were identified by immunostaining with anti-MAP2 antibody (Kitao et al., 2001). Neuronal cell death was assessed by an overlapping distribution of either TUNEL or activated caspase-3 staining and MAP2-positive cells. In each case (studies involving TUNEL assay and immunocytochemistry), two observers without knowledge of the experimental protocol evaluated sections and experiments were repeated at least three times.

Cell culture of cerebellar neurons. Primary cultures of cerebellar cells were prepared from cerebella of mouse pups (embryonic day 18) as described by Netzeband et al. (1999), followed by determination of genotype by PCR (Kitao et al., 2001). In brief, cerebellar cortices were isolated from the surrounding tissue and then minced and triturated without enzymatic treatment in saline containing (in mM): 137 NaCl, 5.4 KCl, 0.17 Na_2HPO_4, 0.22 KH_2PO_4, 33.3 glucose, 43.8 sucrose, and 10 HEPES-NaOH, pH 7.3. Cells were plated on 15 mm round coverslips ($\sim 10^5$ cells per slip) coated with poly-L-lysine (Sigma). Cultures were then placed on a feeder layer of astrocytes, which were incubated in DMEM (Sigma) supplemented with horse serum (heat-inactivated, 10%), fetal calf serum (heat-inactivated, 10%), and glucose (5 gm/l). The medium was exchanged twice weekly, and experiments were performed after cells had been maintained for 9 d *in vitro*.

Assessment of Purkinje cell death in vitro. Purkinje cell death triggered by either excitotoxicity or oxygen deprivation was assessed as described by Brorson et al. (1995). In brief, cells plated on chamber slides were exposed to either AMPA (30 μM; Sigma) or vehicle (PBS) dissolved in HEPES-buffered saline containing tetrodotoxin (0.5 μM) and bicuculline (20 μM) for 20 min, as described (Brorson et al., 1995). After exchange of the medium, cells were further maintained under normoxic conditions for up to 24 hr. To determine cell viability in the setting of oxygen deprivation, cultures were either exposed to hypoxia, using a controlled environment chamber (Ogawa et al., 1990), or maintained in normoxia for up to 24 hr. In each experiment, cultures on chamber slides, treated in the same manner, were immunostained with antibody to calbindin D_{28k}. Calbindin D_{28k}-positive and -negative cells were counted to achieve totals of >100 for each condition by a blinded evaluator. Survival of calbindin D_{28k}-positive neurons under each condition was calculated as relative survival based on the quotient of calbindin D_{28k}-positive cells under that condition divided by calbindin D_{28k}-positive cells present under control conditions. Similarly, the specific survival of calbindin D_{28k}-negative neurons under each condition was calculated as relative survival based on the quotient calbindin D_{28k}-negative cells under that condition divided by calbindin D_{28k}-negative cells under control conditions. No qualititative change in the appearance of the calbindin D_{28k} staining pattern was observed in surviving neurons. Survival of calbindin D_{28k}-positive or -negative cells was determined by at least three separate experiments.

Western blot and analysis. Levels of ORP150 antigen in tissue extracts were determined semiquantitatively by immunoblotting, as described (Kuwabara et al., 1996). Tissue extracts were prepared in PBS containing NP-40 (1%), and proteins were separated by SDS-PAGE and transferred to polyvinylidene difluoride paper, followed by incubation with either anti-human ORP150 antibody (1 μg/ml) or anti-human β-actin antibody (1000× dilution; Sigma), the latter as an internal control. Where indicated, Western blotting using anti-KDEL monoclonal antibody (Stressgen Biotechnologies Co.; 0.2 μg/ml) was used to assess levels of GRP78 (78 kDa glucose-regulated protein; Ozawa et al., 1999). Densitometric evaluation was employed to assess ORP150 antigen using imaging software (Adobe Photoshop).

Behavioral studies. Mice were subjected to behavioral analysis 30 d after birth. After identification of genotypes (see above), animals were subjected to open-field and rotor rod tests. During the open-field test, animals were allowed to search freely in a square acrylic box (30 × 30 cm) for 20 min. The light attached to the sealing of the enclosure was on during the first 10 min (light period) and off during the later 10 min. On each *x* and *y* bank of the open field, two infrared rays were attached 2 cm above the floor at 10 cm intervals, making a flip-flop circuit between the two beams. The total number of beam crossings was counted for 10 min as traveling behavior of the animal (locomotion). On the *x* bank, the other 12 infrared rays were set 5 cm above the floor at 3 cm intervals, and

the total number of beam crossings was counted for 10 min as rearing behavior (rearing). The enclosure was washed with water and then 70% ethanol between each test to avoid the smell, which interferes with mouse behavior. In the rotor rod test, an animal was placed on a drum that was turned at a speed of 2.5 rpm for 30 sec. If the animal fell during the interval, the latency was recorded. If the mouse could maintain its position, the speed was accelerated by 2.5 rpm every 30 sec; i.e., to 5, 7.5, and 10 rpm at 30 sec intervals. Falling latency was then recorded. Each trial was repeated three times, and the mean latency of three trials was calculated for each mouse. Student's *t* test was used for statistical comparison.

Electrophysiological analysis. Parasagittal cerebellar slices (250 μm thickness) were prepared from ORP150 $^{+/-}$, ORP150 $^{+/+}$, or Tg ORP150 mice as described (Kano et al., 1995). Whole-cell recordings were made from visually identified Purkinje cells using an upright microscope (BX50WI; Olympus Optical, Tokyo, Japan) at 31°C. Resistance of patch pipettes was 3–6 MΩ when filled with an intracellular solution composed of (in mM): 60 CsCl, 10 Cs gluconate, 20 TEA-Cl, 20 BAPTA, 4 $MgCl_2$, 4 ATP, and 30 HEPES, pH 7.3, adjusted with CsOH. Pipette access resistance was compensated by 70–80%. Composition of the standard bathing solution was (in mM): 125 NaCl, 2.5 KCl, 2 $CaCl_2$, 1 $MgSO_4$, 1.25 NaH_2PO_4, 26 $NaHCO_3$, and 20 glucose, bubbled with 95% O_2 and 5% CO_2. Bicuculline (10 mM) was always added to block inhibitory synaptic transmission. Ionic currents were recorded with an Axopatch 1D patch-clamp amplifier (Axon Instruments, Foster City, CA). Signals were filtered at 2 kHz and digitized at 20 kHz. On-line data acquisition and off-line data analysis were performed using PULSE software (HEKA). Stimulation pipettes (5–10 mm tip diameter) were filled with standard saline and used to apply square pulses for focal stimulation (duration, 0.1 msec; amplitude, 0–90 V). Climbing fibers were stimulated in the granule cell layer 50–100 mm away from the Purkinje cell soma.

Statistical analyses. Unless indicated otherwise, statistical analysis was performed by either ANOVA followed by multiple-comparison analysis using the Newman–Keuls equation or two-way ANOVA followed by multiple-contrast analysis. Where indicated, data were analyzed by χ^2 analysis.

Results

Expression of ORP150 in developing brain

Immunoblotting was performed to compare levels of ORP150 in different regions of developing mouse brain. Expression of ORP150 in cerebral cortex (Fig. 1*A*), caudate putamen (Fig. 1*B*), and hippocampus (Fig. 1*C*) displayed a small, although nonsignificant, rise from the time of birth to postnatal days 8–20, when an apparent plateau was reached. Immunohistochemical analysis revealed low levels of ORP150 antigen in a range of neurons in the latter brain subregions on postnatal days 1, 4, and 10 (Fig. 1*F–H,K–M,P–R*, respectively). In contrast, ORP150 peaked 4–6 d after birth in cerebellum, with levels significantly above the baseline, by threefold to fivefold, on days 4–8 (Fig. 1*D*). Cerebellar ORP150 antigen detected immunohistochemically showed a parallel rise on postnatal day 4 (Fig. 1*N*) compared with days 1 and 10 (Fig. 1*I,S*). On the basis of Nissl staining of adjacent slices, ORP150 was localized predominantly to the Purkinje cell layer (Fig. 1*T,V*). Consistent with previous reports (Stacchiotti et al., 1997; Calabrese et al., 2002), inducible-type HSP70 was also expressed in the Purkinje cell layer (Fig. 1*U*). Another class of molecular chaperones, GRP78 and GRP94, displayed very low-level expression using anti-KDEL antibody in the cerebellum 4 d after birth (Fig. 1*W*) (Kitao et al., 2001). Expression of stress-related proteins, such as JNK (Urano et al., 2000) and CHOP (Wang et al., 1996), was also virtually undetectable on postnatal day 4 (Fig. 1*X,Y*, respectively).

In view of the role of ORP150 in stress-mediated neuronal cell death (Kitao et al., 2001; Tamatani et al., 2001), we examined whether there was a relationship between ORP150 expression and induction of ORP150 in the developing cerebellum. Immunohistochemical analysis with antibody to activated caspase-3 and TUNEL staining both showed ~2–3% positive neurons (i.e., MAP2-positive cells) in cerebral cortex, caudate putamen, and hippocampus (Fig. 2*A–C*). In contrast, there is an increase in cells labeled with activated caspase-3 antigen, the latter defined as Purkinje cells based on immunoreactivity with calbindin D_{28k} (Brorson et al., 1995), 4–6 d after birth (Fig. 2*D,E–H*). DNA fragmentation, displayed by TUNEL assay, followed the increase in activated caspase-3 antigen (Fig. 2*D,I–L*). These data indicate that ORP150 expression appears to be maximal at a time corresponding to programmed death of Purkinje cells.

Expression of ORP150 in cerebellum in genetically manipulated mice and the effect on Purkinje cell death

Our previous work demonstrated a protective effect of ORP150 on neuronal viability in the settings of ischemia and excitotoxicity. Thus, expression of ORP150 in Purkinje cells at a time corresponding to induction of cell death could denote insufficient expression of endogenous ORP150 to exert a protective effect. Alternatively, the function of ORP150 in the cerebellum might be quite different from what has been observed elsewhere (Tamatani et al., 2001). To address these issues, we turned to genetically manipulated mice: heterozygous for deficiency of ORP150 (ORP150 $^{+/-}$) and heterozygous transgenic with neuronal expression of ORP150 driven by the PDGF B-chain promoter (Tg ORP150).

Immunoblotting was performed to assess ORP150 antigen levels in ORP150 $^{+/-}$, wild-type (ORP150 $^{+/+}$), and Tg ORP150 mice in the cerebellum (Fig. 3). ORP150 $^{+/-}$ animals displayed a relatively constant low level of ORP 150 antigen up to 30 d after birth (Fig. 3*A*), compared with intermediate levels (following the expression pattern observed in Fig. 2*D*) in non-Tg littermates (wild-type; Fig. 3*H*) and constant high levels in Tg ORP150 animals (Fig. 3*P*). The latter were maintained up to postnatal day 120 (data not shown). Immunohistochemical analysis using antibodies to calbindin D_{28k} and ORP150 showed decreased expression of ORP150 antigen in the Purkinje cell layer from ORP150 $^{+/-}$ mice (Fig. 3*B–G*). Non-Tg littermates displayed time-dependent ORP150 induction, peaking at 4–6 d after birth (Fig. 3*I–N*). Tg ORP150 mice displayed uniform and strong staining in the Purkinje cell layer (Fig. 3*Q–V*). The latter high level of ORP150 expression was maintained at the latest time point evaluated, 30 d (data not shown).

The key issue was to correlate levels of ORP150 expression with induction of apoptosis in the Purkinje cell layer, on the basis of TUNEL assay (Migheli et al., 1995) and immunostaining with antibody to activated caspase-3 (Selimi et al., 2000). In ORP150 $^{+/-}$ mice, cell death in the Purkinje cell layer was apparent by TUNEL analysis [Fig. 4*A–C*, postnatal day 6 (P6), P10, arrowheads] and immunohistochemical staining with antibody to activated caspase-3 (Fig. 4*D*, P4, arrowheads). Both TUNEL (Fig. 4*F–H*, arrowheads) analysis and immunostaining (Fig. 4*I*, arrowheads) showed that signals related to Purkinje cell death tended to be fewer in wild-type littermates (OPR150 $^{+/+}$), although this difference was not statistically significant. Such evidence of programmed cell death in wild-type and ORP150 $^{+/-}$ animals was strongly suppressed in Tg ORP150 mice (Fig. 4*K–N*). Image analysis demonstrated a significant reduction in TUNEL- and caspase-3-positive cells from Tg ORP150 animals on days 4–6, compared with wild-type and ORP150 $^{+/-}$ animals (Fig. 4*P,Q*). Even by postnatal day 12, there were greater numbers of TUNEL-positive nuclei in the cerebellum of ORP150 $^{+/-}$ animals compared with wild-type animals (Fig. 4*P*). The sup-

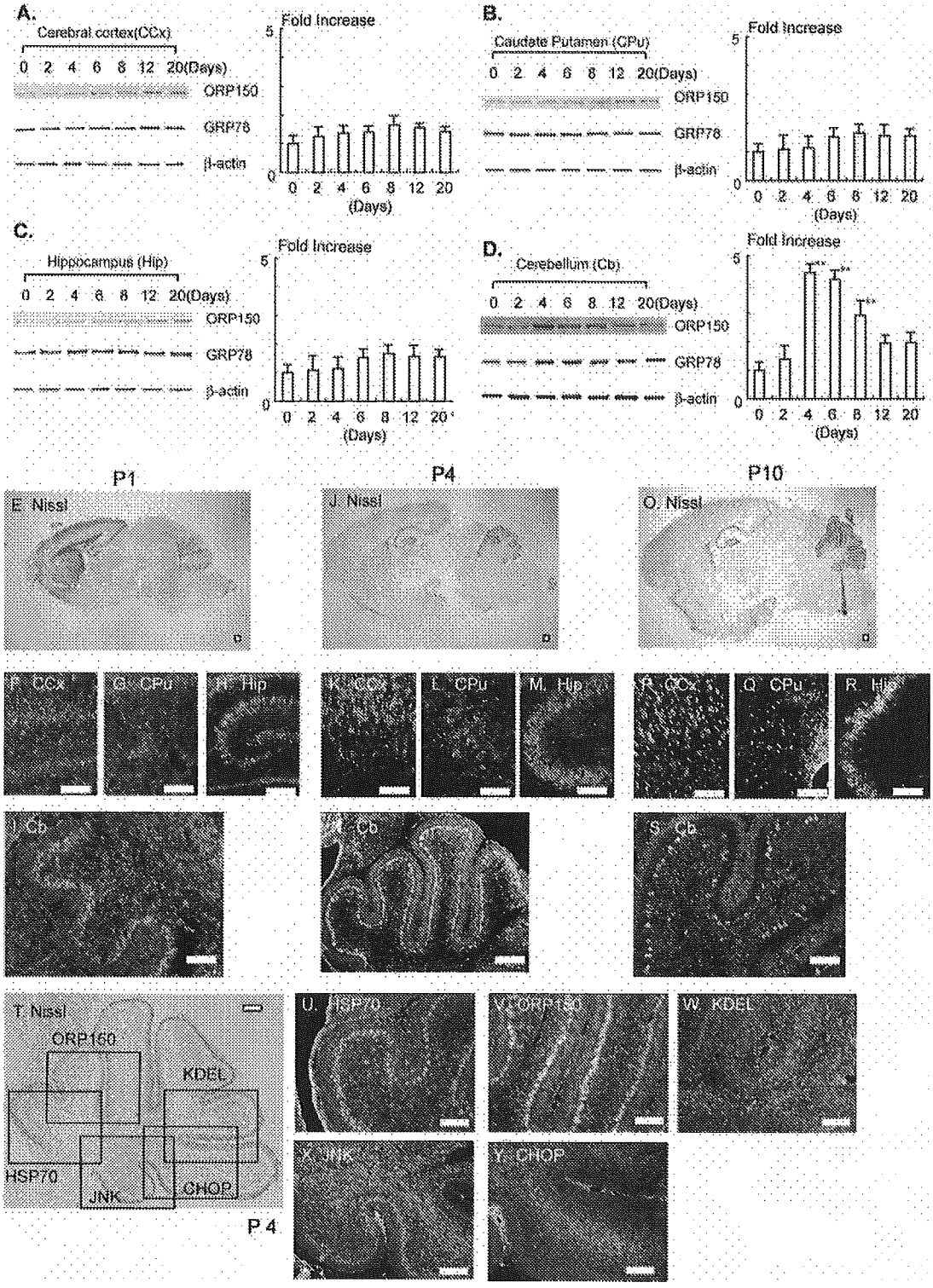

Figure 1. Expression of ORP150 in brain during postnatal development. *A–D*, Protein extracts prepared from cerebral cortex (CCx; *A*), caudate putamen (Cpu; *B*), hippocampus (Hip; *C*), or cerebellum (Cb; *D*) during development (0–20 d after birth) were subjected to Western blotting using antibody to ORP150 (top lanes), GRP78 (middle lanes), or β-actin (bottom lanes). In each blot, densitometric analysis of the ORP150 band intensity was performed and expressed by fold increase versus that on day 0; $n = 6$ per time point. $^{**}p < 0.01$, multiple-comparison analysis followed by ANOVA. *E–S*, Mouse brain was perfusion-fixed on P1, P4, and P10. Tissue was either stained with cresyl violet (*E*, *J*, *O*) or immunostained with antibody to ORP150 (*F–I*, *K–N*, *P–S*). *T–Y*, Mouse brain (P4) was stained with cresyl violet (*T*). Adjacent sections were stained with antibody to inducible-type HSP70 (*U*), ORP150 (*V*), KDEL (which recognizes both GRP78 and GRP94; *W*), activated JNK (*X*), or CHOP (*Y*). Orientation of *U–Y* is indicated as an open box in *T*. Scale bars, 100 μm. Images representative of six experiments are shown.

pression of Purkinje cell death was generally observed in cerebellum because there were no anatomical differences (i.e., vermis or hemisphere) in the frequency of either TUNEL- or activated caspase-3-positive signals (data not shown).

We reasoned that if Tg ORP150 mice displayed strongly attenuated evidence of apoptosis in the Purkinje cell layer, then there might also be a difference in cell number in the cerebellum. The number of calbindin D_{28k}-positive cellular profiles was used to

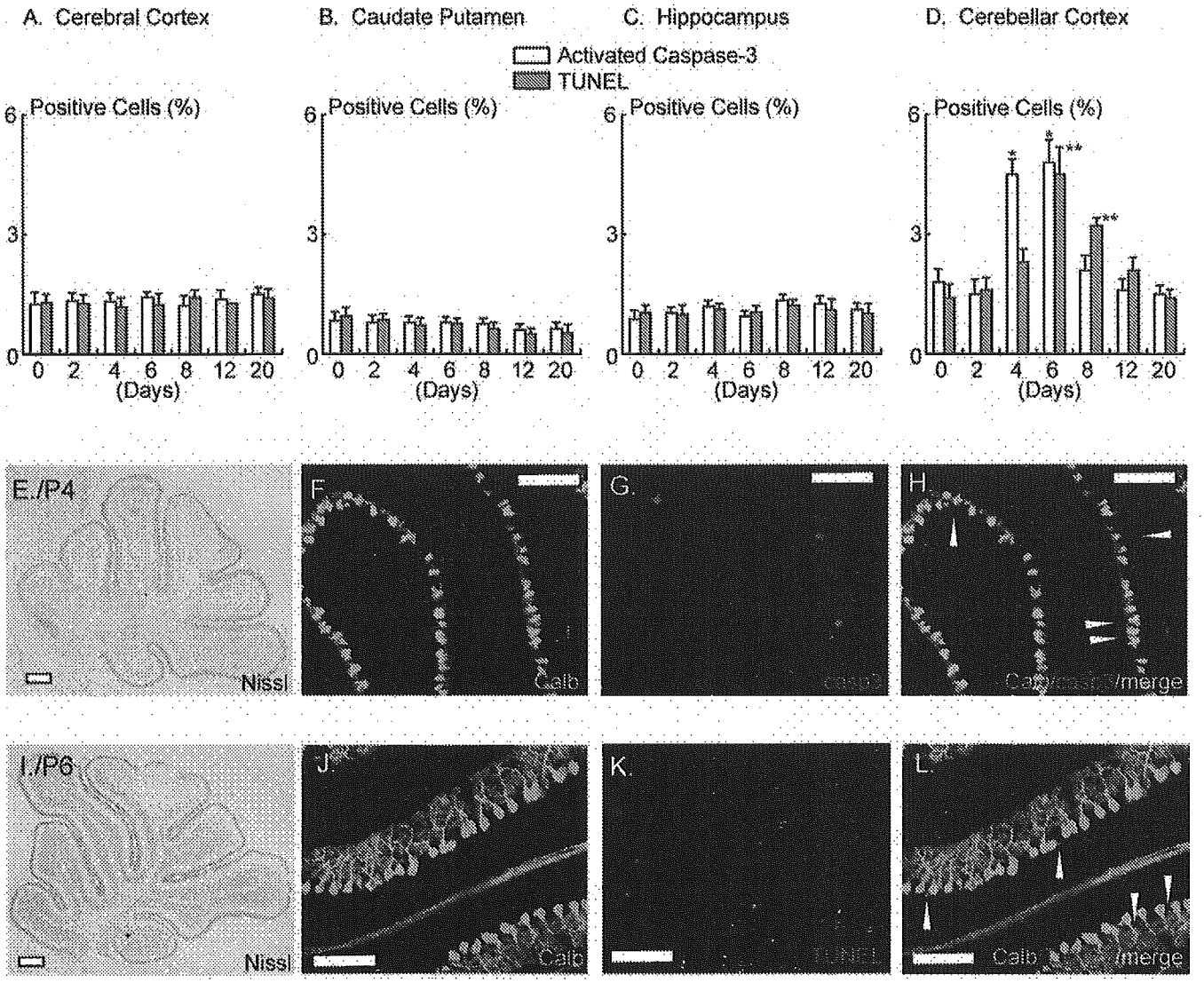

Figure 2. Cell death in the postnatal developing brain. *A–D*, Mouse brain was perfusion-fixed 0–20 d after birth. Cerebral hemispheres were then stained with antibody to activated caspase-3 or by the TUNEL method. The same sections were also visualized with either antibody to MAP2 staining (for *A–C*; data not shown) or calbindin D28K (for *D*; data not shown) to identify neurons (*A–C*) or Purkinje cells (*D*). Open bars represent the percentage of activated caspase-3-positive cells also positive for MAP2 (*A–C*) or calbindin D_{28k} (*D*); shaded bars represent TUNEL-positive cells in each population; $n = 6$ per experimental condition. $^{*,**}p < 0.01$ by multiple-comparison analysis followed by two-way ANOVA, compared with the values at day 0. *E–H*, Cerebellar sections prepared 4 d after birth were stained with cresyl violet (*E*), antibody to calbindin D_{28k} (Calb; *F*), or activated caspase-3 (casp3; *G*). The merged image of *F* and *G* is shown in *H*. *I–L*, Cerebellar sections prepared 6 d after birth were stained with either cresyl violet (*I*), antibody to calbindin D_{28k} (*J*), or using the TUNEL method (*K*). The merged image of *J* and *K* is shown in *L*. Scale bars, 100 μm. Images representative of six experiments are shown.

identify Purkinje cells (Fan et al., 2001). Compared with wild-type controls (arbitrarily assigned a value of 1), there was a significant increase in Purkinje cells in Tg ORP150 mice (~30–40%). In contrast, there was a decrease in Purkinje cells (~20%) in ORP150$^{+/-}$ mice that did not achieve significance. Although assessed in different anatomical regions (Baader et al., 1998), no significant difference was observed in either population or cell size between vermis and hemisphere (data not shown). These data indicate that expression of ORP150 in Purkinje cells appears to have a protective effect in terms of cell death during early development, inconsistent with a previous report, which suggested that overexpression of human bcl-2 suppressed programmed Purkinje cell death (Zanjani et al., 1996). In contrast, there was no significant difference in either numerical density or size of granular cells (data not shown), which was assessed by the protocol described by Kakizawa et al. (2000).

ORP150 suppresses Purkinje cell death *in vitro*

To further analyze the effect of ORP150 on the Purkinje cell response to cell stress, cultured Purkinje cells were exposed to either hypoxia (Fig. 5*A*) or AMPA (Fig. 5*C*) for up to 24 hr, followed by assessment of cell viability using immunohistochemical criteria (Brorson et al., 1995). Incubation of cultured Purkinje cells under hypoxic conditions (Fig. 5*A*) or in the presence of AMPA (Fig. 5*C*) decreased the number of calbindin D_{28k}-positive cellular profiles (compared with untreated controls). Cultures prepared from Tg ORP150 mice displayed relative resistance of calbindin D_{28k}-positive cells to each of these stimuli, compared with Purkinje cells from ORP150$^{+/-}$ or wild-type mice. Although we predicted that there might be a notable difference in the response to stress between calbindin D_{28k}-positive cells from ORP150$^{+/-}$ mice and those from non-Tg mice, the former potentially showing greater vulnerability to cell death

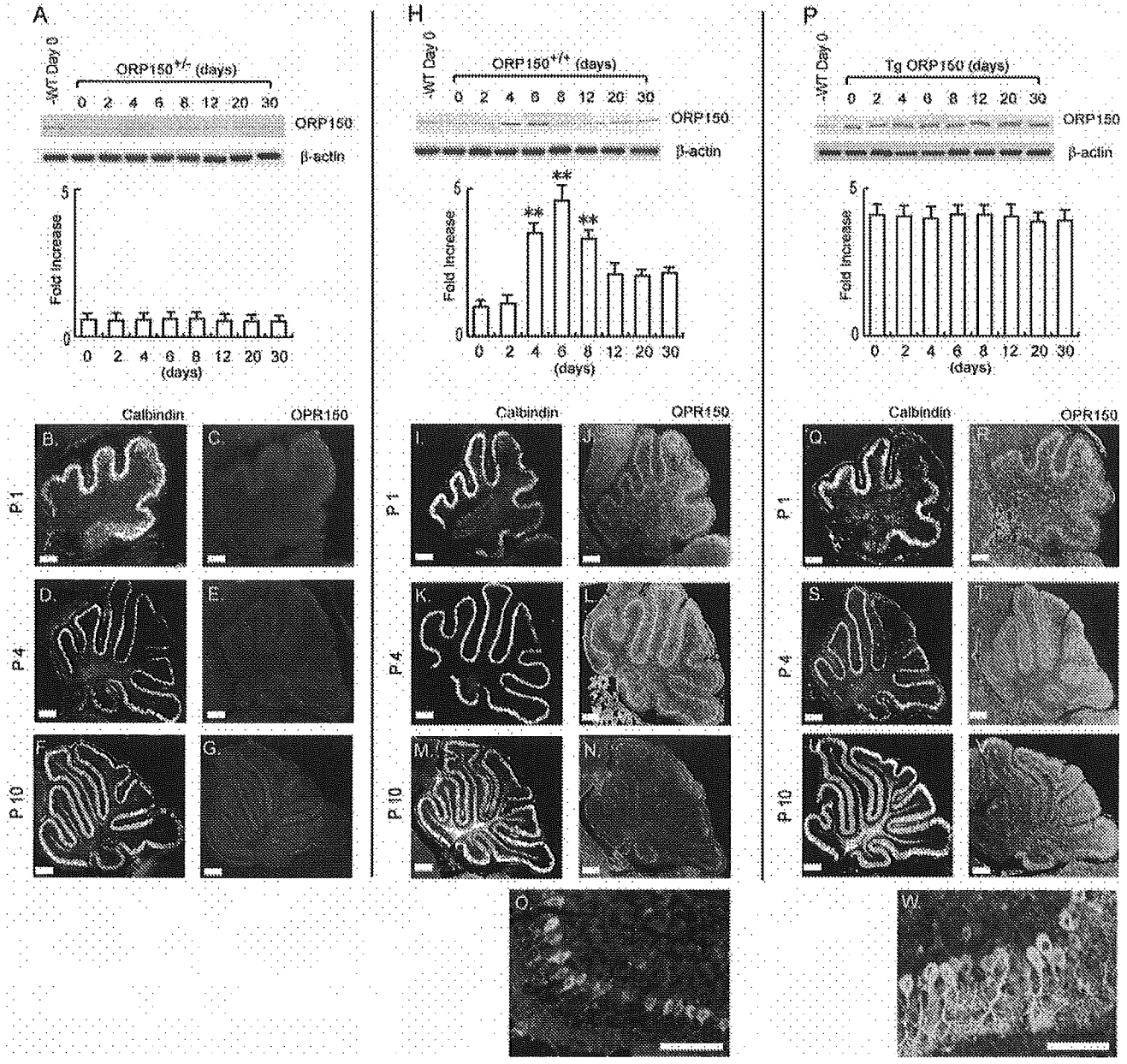

Figure 3. Expression of ORP150 in cerebellum of genetically manipulated mice. Immunoblotting was performed on protein extracts from ORP150 $^{+/-}$ mice (*A*), non-Tg littermates (ORP150 $^{+/+}$; *H*) or Tg ORP150 mice (*P*) at postnatal days 0–30 using antibody to ORP150 (top lanes) or β-actin (bottom lanes). In each panel, densitometric analysis of ORP150 band intensity was performed, and statistical analysis of four representative experiments is shown. Values are expressed as fold increase versus antigen level of ORP150 in the cerebellum in non-Tg littermates at the time of birth; $n = 6$ per time point. $^{**}p < 0.01$, multiple-comparison analysis followed by ANOVA. *B–G*, ORP150 $^{+/-}$ mice were perfusion-fixed at P1, P4, and P10. Cerebellar hemispheres were then subjected to immunostaining using antibody to calbindin D_{28k} (*B, D, F*) or ORP150 (*C, E, G*). *I–O*, ORP150 $^{+/+}$ mice were subjected to immunostaining for calbindin D_{28k} (*I, K, M*) and ORP150 (*J, L, N*) antigen. *O*, Higher magnification of *N*. *Q–W*, Tg ORP150 mice were subjected to immunostaining for calbindin D_{28k} (*Q, S, U*) or ORP150 (*R, T, V*). *W*, Higher magnification of *V*. Scale bar, 100 μm. Images are representative six experiments.

compared with the latter, this difference proved barely discernible in cell culture. Micrographs (Fig. 5*E–J*) of wild-type cultures display representative fields revealing calbindin D_{28k}-positive cells under quiescent conditions (Fig. 5*E,H*) or after exposure to hypoxia (Fig. 5*F*) or AMPA (Fig. 5*I*). Note the evident decrease in calbindin D_{28k}-positive cells in cultures from wild-type animals compared with results using cultures from Tg ORP150 mice (Fig. 5*G,J*).

In contrast, calbindin-negative cells, which mostly represent granular neurons (Brorson et al., 1995), were relatively resistant to both hypoxia (Fig. 5*B*) and AMPA (Fig. 5*D*), regardless of mouse genotype, compared with calbindin D28k-positive neurons. Because expression of ORP150 was similarly decreased in calbindin D_{28k}-positive and -negative neuronal populations *in vitro* from ORP150 $^{+/-}$ mice (data not shown) and similarly increased in calbindin D28k-positive and -negative neuronal populations *in vitro* from Tg ORP150 mice (data not shown), these data suggest a special effect of ORP150 on Purkinje cell viability.

Behavioral and cerebellar function in Tg ORP150 mice

To assess whether suppression of neuronal cell death in Tg ORP150 mice altered cerebellar function in a more global way, behavioral testing was performed using two motor tasks, open-field (Fig. 6*A*) and rotor rod (Fig. 6*B*) tasks (Shahbazian et al.,

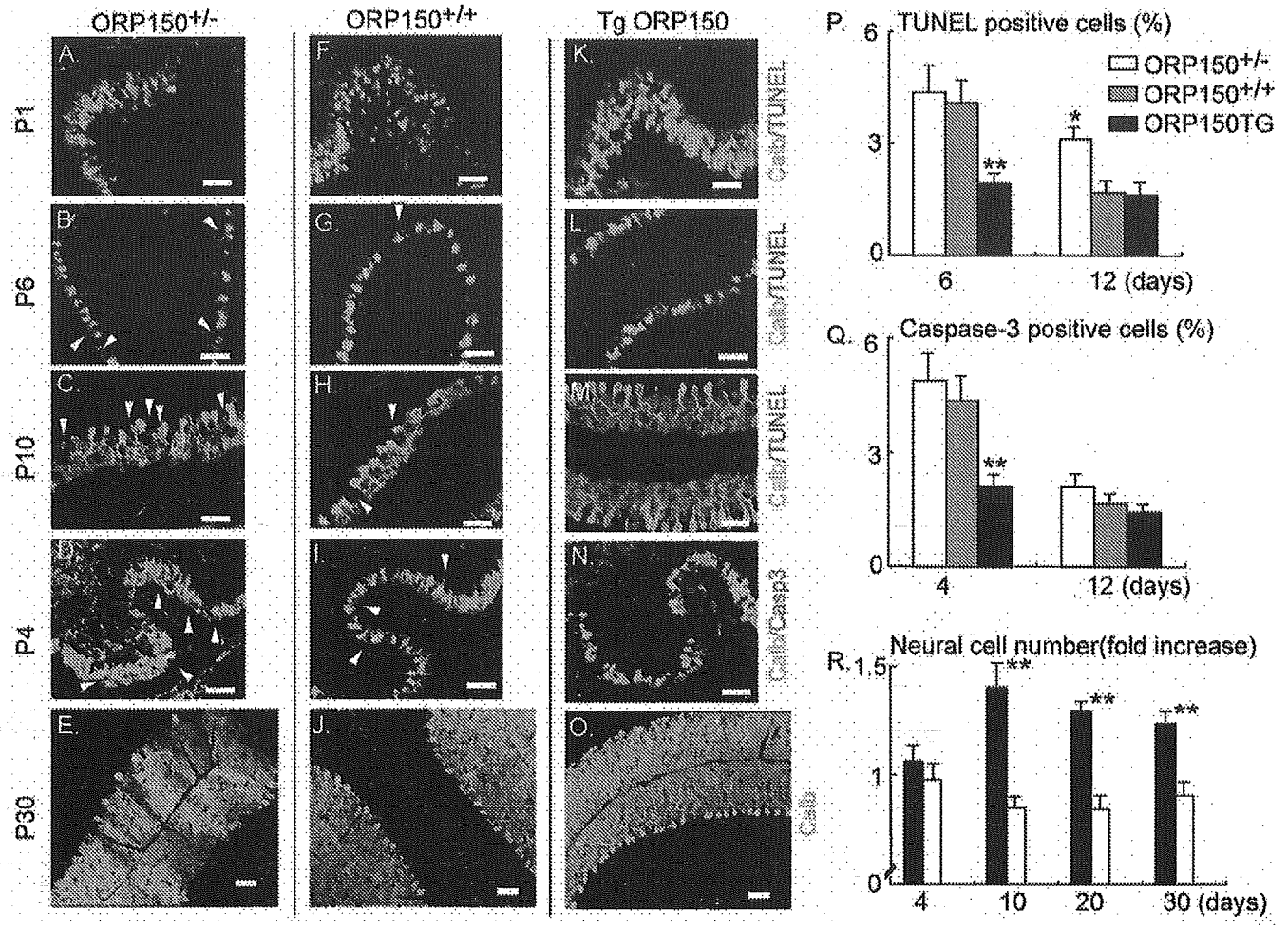

Figure 4. Expression of ORP150 suppresses Purkinje cell death during cerebellar development. *A–O*, ORP150 $^{+/-}$, ORP150 $^{+/+}$, or Tg ORP150 mice were perfusion fixed at P1, P4, P6, P10, and P30 and stained with antibody to calbidin D_{28k} only (Calb; *E, J, O*) or double-stained by TUNEL assay and antibody to calbindin D_{28k} (*A–C, F–H, K–M*), or antibodies to calbindin D_{28k} and activated caspase-3 (Casp3; *D, I, N*). Scale bars, 100 μm; images are representative of six experiments. *P*, The percentage of TUNEL-positive nuclei colocalized with calbindin D_{28k}-positive cells in ORP150 $^{+/-}$ (open bars), ORP150 $^{+/+}$ (shaded bars), or Tg ORP150 (filled bars) mice was determined in samples prepared 6 and 12 d after birth. *Q*, The percentage of cellular profiles positive for both activated caspase-3 and calbindin D_{28k} in ORP150 $^{+/-}$ (open bars), ORP150 $^{+/+}$ (shaded bars), or Tg ORP150 (filled bars) mice was determined in samples prepared 4 and 12 d after birth. $^{**}p < 0.01$; $^{*}p < 0.05$, compared with non-Tg littermates ($n = 6$ per time point). *R*, The population of Purkinje cells (calbindin D_{28k}-positive cells) was counted in the cerebellar hemisphere of Tg ORP150 (filled bars) and ORP150 $^{+/-}$ (open bars) mice at 4, 10, 20, and 30 d after birth. Values are expressed as fold increase or decrease compared with non-Tg littermates; $n = 6$ per time point. $^{**}p < 0.01$, nonpaired *t* test compared with non-Tg (wild-type) littermates.

2001; Chena et al., 2002). In the open-field test (Fig. 6*A*), ORP150 $^{+/-}$ mice displayed performance identical to that of ORP150 $^{+/+}$ animals. In contrast, motor coordination, assessed by the rotor rod test (Fig. 6*B*), showed significant impairment in Tg ORP150 mice. These data suggest that overexpression of ORP150, although enhancing the viability of Purkinje cells in early development and increasing their numbers in adult animals, ultimately caused cerebellar dysfunction. There were no differences in performance of ORP150 $^{+/-}$ and ORP150 $^{+/+}$ mice (data not shown).

Normal cerebellar synaptic function in ORP150 mutant mice

To probe the mechanism underlying cerebellar dysfunction in mutant mice, we examined the electrophysiological properties of Purkinje cells using whole-cell recordings in cerebellar slices. We first compared passive membrane properties of Purkinje cells by recording membrane currents in response to hyperpolarizing voltage steps from the holding potential of −70 to −80 mV. As reported previously (Llano et al., 1991), the decay of the current was biphasic and could be described by the sum of two exponentials (data not shown). From their time constants, we calculated several parameters representing passive properties of Purkinje cells on the basis of the model equivalent circuit of Purkinje cells described by Llano et al. (1991) (Table 1). This model distinguishes two regions in the Purkinje cell. Region 1 represents the soma and the main proximal dendrite, and region 2 represents the main part of dendritic tree. The lumped membrane capacitance of regions 1 and 2 were calculated as C1 and C2, respectively. R1 represents the pipette access resistance. Region 2 is linked to region 1 by resistor R2, which represents the lumped resistance between the main proximal dendrite and each membrane region of the distal dendrites. R3 represents the lumped resistance of the dendritic tree of Purkinje cells. With respect to these parameters, we found no significant differences among ORP150 $^{-/+}$, ORP150 $^{+/+}$, and Tg ORP150 mice (Table 1). These results suggest that the size of the soma and the main proximal dendrite and the extent of the dendritic tree are similar in these three strains of mice.

Purkinje cells receive two distinct excitatory inputs: parallel fibers (the axons of granule cells) and climbing fibers (the axons

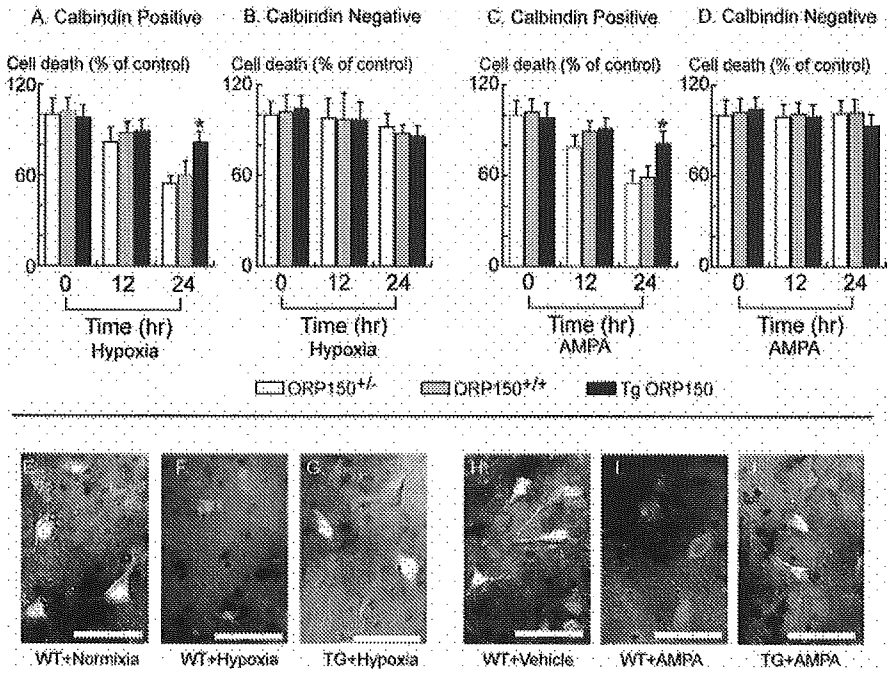

Figure 5. Effect of ORP150 on Purkinje cell death *in vitro*. *A–D*, Purkinje cells were prepared from ORP150 $^{+/-}$ (open bars), ORP150 $^{+/+}$ (shaded bars), or Tg ORP150 (filled bars) mice within 1 d after birth. Cells were then incubated in astrocyte-conditioned medium, as described in Materials and Methods, for 10 d and exposed to hypoxia (*A*, *B*) for 0–24 hr. Viability of Purkinje cells (*A*) and non-Purkinje cells (*B*) was then assessed at the indicated time points, as described in Materials and Methods. Purkinje cells (*C*) and non-Purkinje cells (*D*) were also exposed to AMPA (30 μM) under normoxic conditions. At the indicated time points, cell viability was assessed. Values are expressed as percent cell death compared with the viability of the untreated cultures. *$p < 0.01$, compared with wild-type cultures by multiple-contrast analysis followed by two-way ANOVA. *E–J*, Representative images of immunostaining of cultures from wild-type (WT; non-Tg) animals under controlled conditions, neurons from WT animals exposed to hypoxia (*F*) or AMPA (*I*), or neurons from Tg ORP150 mice (TG) exposed to hypoxia (*G*) or AMPA (*J*). Incubation of cultures under hypoxic conditions (*E*, *F*) or exposure to AMPA (30 μM; *H–J*) was for 24 hr. Scale bars, 100 μm. Images are representative of six experiments.

of the inferior olivary neurons) (Ito, 1984). Individual Purkinje cells are innervated by multiple climbing fibers initially during early development, but supernumerary climbing fibers are pruned subsequently, and most Purkinje cells become monoinnervated by the third postnatal week (Crepel et al., 1981; Mariani and Changeux, 1981a,b). Several knock-out mice show abnormal retention of multiple climbing fiber innervation and impairment of motor coordination (Kano et al., 1995, 1997). Thus, we examined whether multiple climbing fiber innervation persists in the ORP 150 mutant mice. We estimated the number of climbing fibers innervating each Purkinje cell by electrophysiological examination (Kano et al., 1995, 1997). When a climbing fiber was stimulated, an EPSC was elicited in an all-or-none manner in the majority of Purkinje cells (Fig. 6*A*), indicating that such Purkinje cells were innervated by single climbing fibers. In some Purkinje cells, more than one discrete climbing fiber-mediated EPSC (CF-EPSC) could be elicited when the stimulating electrode was moved systematically by 20 μm steps and the stimulus intensity was increased gradually at each stimulation site. The number of climbing fibers innervating the Purkinje cell was estimated by counting the number of discrete CF-EPSC steps. The summary graph in Figure 6*B* indicates that frequency distribution of Purkinje cells in terms of the number of CF-EPSC steps (Fig. 6*A*,*B*) showed no significant difference between the three genetically manipulated mice ($p > 0.05$, χ^2 test). These results suggest that developmental elimination of surplus climbing fibers is normal in these mice. We then examined basic electrophysiological properties of EPSCs by stimulating climbing fibers and parallel fibers. We first examined the kinetics of CF-EPSCs. The 10–90% rise times, decay time constants, and amplitudes were similar among the three strains of mice (data not shown). We then examined short-term plasticity of climbing fiber and parallel fiber synapses. In normal external calcium concentration (2 mM), CF-EPSCs display depression, whereas parallel fiber-mediated EPSCs (PF-EPSCs) undergo facilitation, to the pair of stimuli (Konnerth et al., 1990; Aiba et al., 1994). The paired pulse depression of CF-EPSCs (pulse interval, 10–3000 msec) and the paired pulse facilitation of PF-EPSCs (pulse interval, 10–300 msec) were similar among the three strains of mice (data not shown). These results indicate that basic properties of CF- and PF-EPSCs are normal in these mice.

Discussion

Integral to development of the central nervous system is loss of a large number of neurons through "naturally occurring cell death," by mechanisms that remain to be elucidated (Calabrese et al., 2002). Morphological evidence suggests that such cell death often displays characteristics typical of apoptosis as a final common pathway. However, the key issue is to identify endogenous triggers and breaks on this system that enable selected neuronal populations to survive and to form complex synaptic networks, whereas others are eliminated. Expression of molecular chaperones in developing brain, such as ORP150, suggests the presence of ongoing neuronal stress probably attributable, in part, to perturbations in the local environment. ORP150 was first identified as a stress protein in astrocytes exposed to severe hypoxia (Kuwabara et al., 1996). Because ORP150 is localized to the ER and expressed in response to stress, upregulation of Purkinje cell ORP150 suggests the presence of an ongoing stress response during cerebellar development.

Molecular chaperones are abundant, well conserved proteins essential for maintaining cellular function (Wynn et al., 1994). Environmental stress focused on the ER (termed ER stress) causes a proteotoxic insult: immature proteins accumulate in the ER; conformational changes occur (Patil and Walter, 2001); and induction of molecular chaperones is the result. The protective role of chaperones is crucial for cell survival and repair in response to environmental challenge. In this context, we have previously demonstrated that ORP150 has neurotrophic properties in a range of settings, including ischemia-induced cell death (Tamatani et al., 2001), excitotoxicity (Kitao et al., 2001), and delayed neuronal cell death (Miyazaki et al., 2002). In this article, we have extended this concept by showing that expression of ORP150 in Purkinje cells decreases their vulnerability to hypoxic and excitotoxic stress and enhances their survival during development *in vivo*.

Certain neuronal populations display selective vulnerability to toxic insults, potentially resulting in loss of those cells. Purkinje cells, in particular among cerebellar neurons, are suscepti-

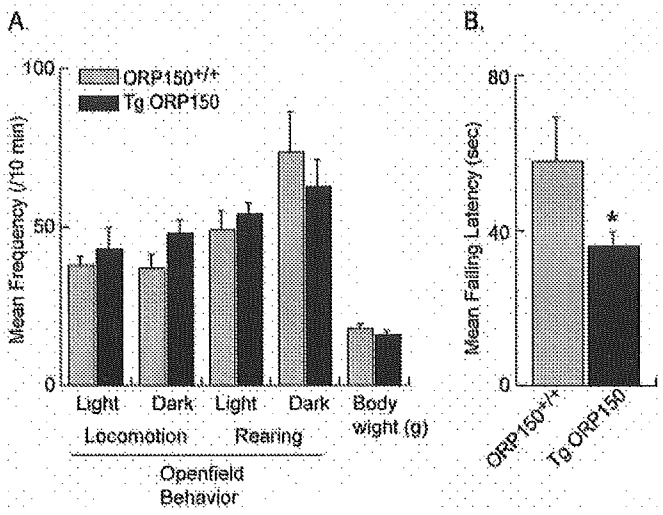

Figure 6. Behavioral analysis of Tg ORP150 mice. Open-field activity (*A*) and rotor rod behavior (*B*) were assessed in non-Tg littermates (ORP150 $^{+/+}$; shaded bars) and Tg ORP150 mice (filled bars). *A*, Open-field performance was examined using an acrylic box as described in Materials and Methods. The total number of crossings across the two infrared rays attached 2 cm above the floor on each *x* and *y* bank was counted during first 10 min (with light on; Light) and the following 10 min (with the light off; Dark) as traveling behavior of the animal (Locomotion). The total number of crossings across the 12 infrared rays attached 5 cm above the floor on the *x* bank was counted during the first 10 min (Light) and the following 10 min (Dark) as rearing behavior of the animal (Rearing). Values are expressed as mean frequency of each activity in each period. Body weights of phenotype mice are also shown at the right. *B*, Motor coordination was evaluated by the mean of falling latency from the rotor rod using an acceleration protocol (2.5, 5, and 7.5 rpm followed by 10 rpm for 30 sec each). Values are mean ± SE. ORP150 $^{+/+}$, $n = 9$ for each condition; Tg ORP150, $n = 6$ for each condition. $^*p < 0.05$, Student's *t* test.

ble to ischemic stress (Sieber et al., 1995; Yoshida et al., 2002), as well as other neurodegenerative-associated conditions (Dove et al., 2000). A likely final common pathway for such toxicity is elevation of free $[Ca^{2+}]i$. Increased $[Ca^{2+}]i$ is associated with a number of cytotoxic events, including chronic ethanol intoxication (Netzeband et al., 1999), diseases characterized by accumulation of proteins with polyglutamine repeats (Clark and Orr, 2000), and traumatic brain injury (Netzeband et al., 1999). Molecular chaperones in the ER have the capacity to function as a buffer system to suppress elevated $[Ca^{2+}]i$ by the maintaining the complex metabolic and biosynthetic properties of this organelle (Yu et al., 1999). In this context, we have demonstrated that ORP150 also suppresses elevations of $[Ca^{2+}]i$ in cultured hippocampal neurons exposed to excitatory amino acids (Kitao et al., 2001). Our preliminary observations reveal expression of ORP150 in Purkinje cells in the setting of human stroke and a primate model of experimental brain ischemia. Taken together, these observations further support the concept that expression of ORP150 in Purkinje cells during development (P4–P8; Figs. 1, 2) is indicative of the presence of environmental stress, potentially ischemic, excitotoxic, or both (see below).

Our current results demonstrate selective upregulation of ORP150 in the developing cerebellum, whereas levels of other molecular chaperones, such as GRP78, remain unchanged. From an evolutionary point of view, these two stress proteins (ORP150 and GRP78) have overlapping functions in yeast. Null mutant strains of lumenal Hsp seventy (LHS)1, the yeast homolog of ORP150, display "compensatory" upregulation of Kar2p, the yeast homolog of GRP78. Although each gene alone is not essential for yeast viability, lethality is observed when inactivating mutations are introduced into both Kar2p and LHS1 (Craven et al., 1996). In contrast, our previous study demonstrated embryonic lethality in homozygous ORP150 $^{-/-}$ embryos (in which the ORP150 gene had been deleted by homologous recombination and replaced by an inactive, truncated form). Thus, it appears that properties of ORP150 and GRP78 have diverged over time; the function of ORP150 cannot be complemented by increased expression of GRP78, and ORP150 appears to be essential for survival in mammalian embryogenesis (Craven et al., 1996). A similar critical role for the HSP47, another molecular chaperone in the ER, in embryonic development has been shown; a genomic mutant of HSP47 also results in embryonic lethality (Nagai et al., 2000).

Mechanisms underlying the vulnerability of cerebellar Purkinje cells to environmental stress remain to be clarified. Cell differentiation and synaptogenesis in cerebellum come in different waves depending on the neuronal populations and afferents and are highly interactive mutually (Altman and Bayer, 1997). In rats, the first postnatal wave comes at P4, characterized with rapid growth in cortex. Most PCs were already multiply innervated by CFs as early as 3 d. The multiple innervation culminated on P5, which rapidly regressed later on (Zhao et al., 1998; Miranda-Contreras et al., 1999). Our results demonstrate increased Purkinje cell death at P4–P6. Though the synaptic formation of climbing fibers from the inferior olive are still immature and confined in somatic regions (Altman and Bayer, 1997), strong immunostaining of glutamate receptor subunits 2 and 3 could be observed at postnatal days 1–3 within Purkinje cell bodies and primary dendrites (Bergmann et al., 1996; Hafidi and Hillman, 1997). At this stage of development, vesicular glutamate transporter is expressed in terminals around PC soma at P1–P10 (Miyazaki T et al., 2003). Because this transporter mainly mediates the filling of cytoplasmic glutamate into synaptic vesicles in terminals, its expression indicates that glutamate release at CF → PC synapses is functional from the molecular point of view, suggesting that polyinnervation of CFs during the first postnatal week could be glutamate stress to developing PCs. A certain extent of Purkinje cell death at this point in development appears to be essential for optimal cerebellar function. Although synaptic properties of Purkinje cells in Tg ORP150 mice appeared normal (Fig. 7), and the number of these neurons was increased (Fig. 4), cerebellar function was clearly suboptimal (Fig. 6). Thus, it is possible that the agility with which certain neuronal populations mount an ER stress response may have important implications for their vulnerability to a range of environmental perturbations.

Table 1. Passive membrane properties of PCs

Mice	C1 (pF)	C2 (pF)	R1 (MΩ)	R2 (MΩ)	Rm (R3) (MΩ)	*n*
ORP150 $^{-/+}$	162.2 ± 87.4	847.6 ± 203.4	6.4 ± 1.1	9.0 ± 2.8	181.5 ± 70.6	16
ORP150 $^{+/+}$	154.8 ± 68.7	870.7 ± 230.9	6.1 ± 0.9	8.0 ± 2.5	162.7 ± 70.8	25
Tg ORP150	171.6 ± 78.1	854.0 ± 120.9	6.3 ± 1.6	7.9 ± 1.9	198.7 ± 88.6	11

Parameters for passive membrane properties were calculated according to the model described by Llano et al. (1991), which distinguishes two regions of Purkinje cells: region 1 representing the soma and the main proximal dendrites and region 2 representing the dendritic tree. C1 and C2 represent the lumped membrane capacitance of regions 1 and 2, respectively. R1 represents the pipette access resistance. Region 2 is linked to region 1 by resistor R2, which represents the lumped resistance between the main proximal dendrite and each membrane region of the distal dendrites. R3 represents the lumped resistance of the dendritic tree of PCs.

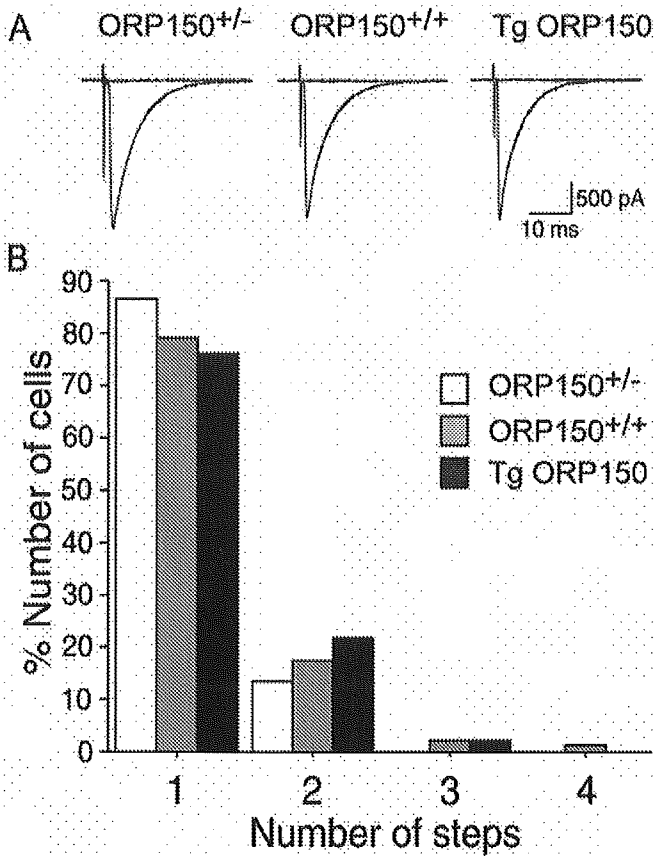

Figure 7. CF innervation of Purkinje cells in ORP150 genetically manipulated mice. *A*, Sample traces of CF-EPSCs recorded from ORP150 $^{+/-}$, ORP150 $^{+/+}$, and Tg ORP150 Purkinje cells. CFs were stimulated in the granular layer at 0.2 Hz, holding the potential at −20 mV. Two or three traces are superimposed at threshold stimulus intensity. *B*, Summary histograms showing the number of discrete steps of CF-EPSCs for ORP150 $^{+/-}$ (open columns; $n = 45$), ORP150 $^{+/+}$ (shaded columns; $n = 91$), and Tg ORP150 (filled columns; $n = 46$) Purkinje cells. There was no significant difference in the distributions for the three types of Purkinje cells ($p < 0.05$, χ^2 test for independent samples).

Consistent with this concept, mutations in the presenilin-1 gene, a cause of familial Alzheimer's disease, also renders neurons more sensitive to glutamate stress (Guo et al., 1999), probably via modification of the ER stress response (Katayama et al., 1999).

We have demonstrated that expression of ORP150 in developing brain most likely serves a cytoprotective function in Purkinje cells. Levels of ORP150 induced during brain development are carefully balanced to allow the appropriate amount of Purkinje cell death but to preserve the necessary number of these cerebellar neurons for normal function. The subtle nature of the system was revealed by overexpression of the ORP150 transgene in Purkinje cells; the number of Purkinje cells increased in Tg ORP150 animals, but cerebellar function was suboptimal. These observations with ORP150 emphasize the importance of ER stress in the Purkinje cell response to ischemia and, most likely, a range of environmental perturbations. It is intriguing to speculate that the same mechanisms that may contribute to neuronal vulnerability to ischemia and excitotoxicity (and, potentially, other stresses), such as insufficient induction of ORP150 to uniformly prevent cell death in the larger population of neurons, may be carefully programmed to prevent excess cell survival during development, at which time such additional neurons would compromise brain function.

References

Aiba A, Kano M, Chen C, Stanto ME, Fox GD, Herrup K, Zwingman TA, Tonegawa S (1994) Deficient cerebellar long-term depression and impaired motor learning in mGluR1 mutant mice. Cell 79:377–388.

Altman J, Bayer SA (1997) An overview of the postnatal development of the rat cerebellum. In: Development of the cerebellar system (Altman J, Bayer SA, eds), pp 317–324. Boca Raton, FL: CRC.

Baader SL, Sanlioglu S, Berrebi AS, Parker-Thornburg J, Oberdick J (1998) Ectopic overexpression of engrailed-2 in cerebellar Purkinje cells causes restricted cell loss and retarded external germinal layer development at lobule junctions. J Neurosci 18:1763–1773.

Bergmann M, Fox PA, Grabs D, Post A, Schilling K (1996) Expression and subcellular distribution of glutamate receptor subunits 2/3 in the developing cerebellar cortex. J Neurosci Res 43:78–86.

Brorson JR, Manzolillo PA, Gibbons SJ, Miller RJ (1995) AMPA receptor desensitization predicts the selective vulnerability of cerebellar Purkinje cells to excitotoxicity. J Neurosci 15:4515–4524.

Calabrese V, Scapagnini G, Ravagna A, Giuffrida Stella AM, Butterfield DA (2002) Molecular chaperones and their roles in neural cell differentiation. Dev Neurosci 24:1–13.

Chena Z, Ljunggrenb HG, Bogdanovica N, Nennesmoc I, Winblada B, Zhu J (2002) Excitotoxic neurodegeneration induced by intranasal administration of kainic acid in C57BL/6 mice. Brain Res 931:135–145.

Clark HB, Orr HT (2000) Spinocerebellar ataxia type 1: modeling the pathogenesis of a polyglutamine neurodegenerative disorder in transgenic mice. Neuropathol Exp Neurol 59:265–270.

Coyle JT, Puttfarchen P (1993) Oxidative stress, glutamate, and neurodegenerative disorders. Science 262:689–695.

Craven RA, Egerton M, Stirling CJ (1996) A novel Hsp70 of the yeast ER lumen is required for the efficient translocation of a number of protein precursors. EMBO J 15:2640–2650.

Crepel F, Delhaye-Bouchaud N, Dupont JL (1981) Fate of the multiple innervation of cerebellar Purkinje cells by climbing fibers in immature control, x-irradiated and hypothyroid rats. Brain Res 227:59–71.

Dove LS, Nahm SS, Murchison D, Abbott LC, Griffith WH (2000) Altered calcium homeostasis in cerebellar Purkinje cells of leaner mutant mice. J Neurophysiol 84:513–524.

Fan H, Favero M, Vogel MW (2001) Elimination of Bax expression in mice increases cerebellar Purkinje cell numbers but not the number of granule cells. J Comp Neurol 436:82–91.

Guo Q, Fu W, Sopher BL, Miller MW, Ware CB, Martin GM, Mattson MP (1999) Increased vulnerability of hippocampal neurons to excitotoxic necrosis in presenilin-1 mutant knock-in mice. Nat Med 5:101–106.

Hafidi A, Hillman DE (1997) Distribution of glutamate receptors GluR 2/3 and NR1 in the developing rat cerebellum. Neuroscience 81:427–436.

Hata R, Matsumoto M, Hatakeyama T, Ohtsuki T, Handa N, Niinobe M, Mikoshiba K, Sakaki S, Nishimura T, Yanagihara T, Kamada T (1993) Differential vulnerability in the hindbrain neurons and local cerebral blood flow during bilateral vertebral occlusion in gerbils. Neuroscience 56:423–439.

Ito M (1984) The cerebellum and neural control. New York: Raven.

Kakizawa S, Yamasaki M, Watanabe M, Kano M (2000) Critical period for activity-dependent synapse elimination in developing cerebellum. J Neurosci 20:4954–4961.

Kano M, Hashimoto K, Chen C, Abeliovich A, Aiba A, Kurihara H, Watanabe M, Inoue Y, Tonegawa S (1995) Impaired synapse elimination during cerebellar development in PKC gamma mutant mice. Cell 83:1223–1231.

Kano M, Hashimoto K, Kurihara H, Watanabe M, Inoue Y, Aiba A, Tonegawa S (1997) Persistent multiple climbing fiber innervation of cerebellar Purkinje cells in mice lacking mGluR1. Neuron 18:71–79.

Katayama T, Imaizumi K, Sato N, Miyoshi K, Kudo T, Hitomi J, Morihara T, Yoneda T, Gomi F, Mori Y, Nakano Y, Takeda J, Tsuda T, Itoyama Y, Murayama O, Takashima A, St. George-Hyslop P, Takeda M, Tohyama M (1999) Presenilin-1 mutations downregulate the signalling pathway of the unfolded-protein response. Nat Cell Biol 1:479–485.

Kitao Y, Ozawa K, Miyazaki M, Tamatani M, Kobayashi T, Yanagi H, Okabe M, Ikawa M, Yamashima T, Tohyama M, Stern D, Hori O, Ogawa S (2001) Expression of 150 kda oxygen regulated protein (orp150), a molecular chaperone in the endoplasmic reticulum, rescues hippocampal neurons from glutamate toxicity. J Clin Invest 108:1439–1450.

Konnerth A, Llano I, Armstrong CM (1990) Synaptic currents in cerebellar Purkinje cells. Proc Natl Acad Sci USA 87:2662–2665.